# The Binding Ability of Iron Bonded to Porphodimethene: Structural, Magnetic, and Electronic Relationship to Iron Porphyrin Complexes

**Carlos Da Silva,[a] Lucia Bonomo,[a] Euro Solari,[a] Rosario Scopelliti,[a] Carlo Floriani,*[a] and Nazzareno Re[b]**

**Abstract:** The availability of the parent compound, *meso*-hexaethylporphodimetheneiron(II), [($Et_6N_4$)Fe] (**2**), of this report results from a novel synthetic methodology that makes [$Et_6N_4Li_2$] (**1**) easily available. The major focus is on how the axial positions, which are the key reactive sites in metalloporphyrins, and the electronic configuration of the metal can be affected by the breakdown of the aromaticity of the porphyrin skeleton and by the nonplanar conformation of the ligand. DFT calculations indicate a $^3B_1(d_{z^2})^1(d_{yz})^1$ ground state for **2** versus the $^3A_2(d_{xz})^1(d_{yz})^1$ ground state in the porphyrin analogue. The intermediate-spin state ($S=1$) of **2** changed drastically upon addition of one or two axial ligands, as hexacoordination is preferred by iron(II). The hexacoordinate complexes [($Et_6N_4$)Fe(L)(L′)] (L = L′ = THF, **3**; L = L′ = Py, **4**; L = PhNO, L′ = Py, **14**) have been isolated and structurally characterized. Strong-field ligands lead to a low-spin diamagnetic state for iron(II), namely for complexes **4**–**7**, **9**, and **14**, whereas **3** is a typical $d^6$ high-spin complex, as is the pentacoordinate [($Et_6N_4$)Fe(CN)]$Bu_4N$ (**8**). The structural analysis showed common features for **6**, **7**, **9**, and **14**: i) a small displacement of the metal from the $N_4$ plane, and ii) an $N_4$ cavity, larger than that in the corresponding porphyrins, affecting the Fe–N bond lengths. The $^1$H NMR spectrum is quite diagnostic of the two-fold symmetry in the diamagnetic hexacoordinate complexes, revealing either a $D_{2h}$ or a $C_{2v}$ symmetry. The CO stretching frequency (1951 $cm^{-1}$) in complex **6** probes the good electron density at the metal. The one-electron oxidation of **2** led to pentacoordinate iron(III) derivatives [($Et_6N_4$)Fe(Cl)] (**10**), [($Et_6N_4$)$_2$$Fe_2$($\mu$-O)] (**11**), and [($Et_6N_4$)$_2$-$Fe_2$($\mu$-*p*-$OC_6H_4$-O)] (**12**). Complex **10** is a typical high-spin iron(III) (5.85 $\mu_B$ at 298 K), while **11** and **12** behave as antiferromagnetic coupled iron(III) ($J=-9.4$ $cm^{-1}$, **12**, and $J=-115$ $cm^{-1}$, **11**). In complexes **10**, **11**, and **12** iron is sitting in a quite distorted square pyramidal geometry, in which the ligand displays a very distorted roof conformation with different degrees of ruffling. Distinctive structural and magnetic features have been found for the nitrosyl derivative [($Et_6N_4$)Fe–NO], which has a low-spin state ($S=1/2$) and the following structural parameters: Fe–N–O, 147.3(2)°; Fe–N, 1.708(2) Å; N–O, 1.172(3) Å. A comparative structural, magnetic, and theoretical analysis of the compounds listed above has been made with the analogous porphyrin derivatives. The detailed structural investigation has been mapped through the X-ray analysis of **2**, **7**, **8**, **9**, **11**, **13**, and **14**.

**Keywords:** coordination modes · iron · magnetic properties · porphodimethene · porphyrinogens · redox chemistry

## Introduction

A porphodimethene skeleton paves the way from porphyrinogen to porphyrin, being formally the four-electron oxidation product of porphyrinogen (Scheme 1),[1, 2] but its tetrapyrrolic structure has not had, so far, much success as a metal-binding macrocycle. This was mainly due to the quite difficult synthetic access, that went through the reductive alkylation of the corresponding porphyrin.[3] Such a synthetic method has a number of severe limitations, namely: i) the use of metallated

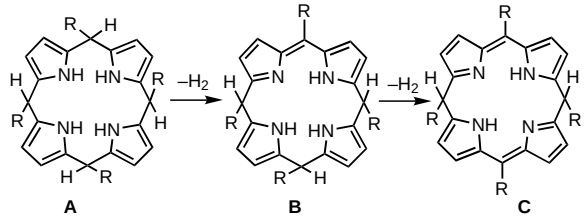


Scheme 1. The two- and four-electron oxidation of porphyrinogen **A** to porphomethene **B** and porphodimethene **C**.

[a] Prof. Dr. C. Floriani, C. Da Silva, L. Bonomo, Dr. E. Solari, Dr. R. Scopelliti
Institut de Chimie Minérale et Analytique, Université de Lausanne
BCH, 1015 Lausanne (Switzerland)
Fax: (41) 21-692-3905
E-mail: carlo.floriani@icma.unil.ch

[b] Prof. N. Re
Facoltà di Farmacia, Università degli Studi G. D'Annunzio
66100 Chieti (Italy)

Supporting information for this article is available on the WWW under http://www.wiley-vch.de/home/chemistry/ or from the author.



0947-6539/00/0624-4518 $ 17.50+.50/0

forms of the porphyrin; ii) the use of sterically hindered porphyrins, like the octaalkyl derivatives; and iii) the limited scale at which the synthesis can be performed. Also a recently reported method is unpracticable,[4] since it does not allow the synthesis to be scaled up and the porphodimethenes remain synthetic curiosities. Finally, a novel methodology has made available a large-scale synthesis of the porphodimethene skeleton in the protic form, as well as a lithium derivative, which is particularly appropriate for transmetallation reactions.[5] Porphodimethene as a macrocyclic ligand has peculiar features that places it inbetween porphyrinogen and porphyrin. It would serve to test how much the changes in the aromaticity, the conformation of the ligand, and the electronic properties can affect the binding ability of the metal towards the substrates, which has been so extensively studied in metal porphyrin chemistry. This report deals with an extensive exploration of the synthesis and reactivity of *meso*-hexaethylporphodimetheneiron(II).[6] The structural, magnetic, and theoretical analysis of iron(II) and iron(III) derivatives allows a quite interesting comparison to be made for the metal behavior in the corresponding iron porphyrin complexes.

## Results and Discussion

Results and discussion will be presented in three separate sections: i) synthesis and reactivity, ii) structural studies, and iii) magnetic and theoretical studies, thus effecting the comparison within the same class of compounds and with analogous porphyrin derivatives.

**Synthesis and reactivity:** The synthesis of the parent compound **2** was achieved by the transmetallation of **1** in benzene (Scheme 2). The reaction led to the formation of green crystals of **2**, which have a magnetic moment of 3.65 $\mu_B$ at 298 K. Complex **2** is quite soluble in hydrocarbons and polar solvents and is oxygen sensitive.

The first class of reactions to which complex **2** was exposed was the axial coordination of different substrates. Regardless of the nature of the coordinating solvent, complex **2** always achieved hexacoordination, as exemplified by complexes **3** and **4**. Attempts to synthesize five-coordinate iron derivatives by using an appropriate stoichiometric ratio or the reaction between **2** and the bis-solvated form were completely unsuccessful. The nature of the axial ligand particularly affects the magnetic state of the iron(II), moving from a paramagnetic species, complex **3**, to a fully diamagnetic species, complex **4**, which can easily be characterized by $^1$H NMR spectroscopy. According to a two-fold symmetry, two doublets for the $\beta$-protons of the pyrroles and two different kind of ethyl groups, in accordance with a $D_{2h}$ symmetry, were observed. In the case of a strong π-acid, such as carbon monoxide, only a very labile *trans*-dicarbonyl ($\nu_{CO} = 2021.6$ cm$^{-1}$) was obtained, as monitored by a gas-volumetric experiment. The attempt to isolate **5** in the solid state led only to the starting material. Axial coordination in metalla-porphyrins is the way to get activation and transformation of the substrate.[7] In order to remove the reciprocal *trans* labilization of the two CO molecules, carbonylation was carried out in the presence of pyridine, which has the appropriate synergetic σ donation to stabilize the carbon monoxide in the *trans* position. This is proven by the rather low CO stretching frequency at 1951.6 cm$^{-1}$ in **6**, compared with that of 2021.6 cm$^{-1}$ in **5**.

The prevailing σ-donation from *t*BuNC led to the formation of the diamagnetic bis-isocyanide derivative **7** ($\nu_{CN} =$ 2113.3 cm$^{-1}$) exclusively, regardless of the stoichiometric ratio employed. The rather high stretching frequency is in agreement with a competitive π back-donation to the two isocyanides. The $^1$H NMR spectrum is in agreement with the $D_{2h}$ symmetry of the complex. Once more, *trans* self-labilization was observed in the reaction of **2** with $Bu_4N^+CN^-$, leading exclusively to the monocyanide derivative **8**. Its stretching frequency ($\nu_{CN} = 2049.2$ cm$^{-1}$) is lowered to 1965.8 cm$^{-1}$ when iron binds a σ donor, like pyridine, in the axial position *trans* to the cyanide, complex **9**. In the meantime, we moved from a paramagnetic complex, complex **8** ($\mu_{eff} = 4.72\ \mu_B$ at 298 K), to a diamagnetic one, complex **9**. In the case of cyanide, we were unable to detect, in either the solid state or in solution, any further binding of $CN^-$ to form a hexacoordinated iron(II), though such an equilibrium was very often observed in iron(III) porphyrin complexes.[7a, 7b]

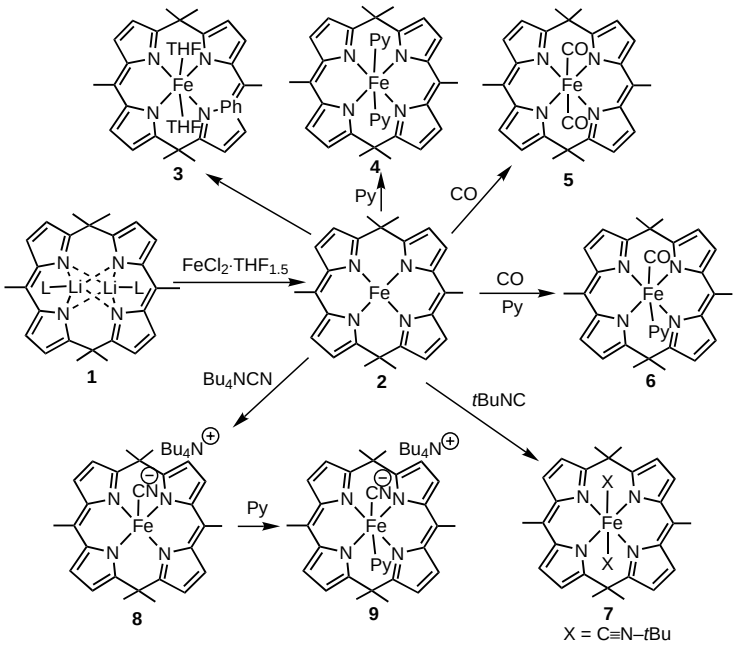


Scheme 2. The axial coordination of hexaethylporphodimetheneiron(II) (**2**) to give the corresponding iron(III) derivatives.

  0947-6539/00/0624-4519 $ 17.50+.50/0 

The reactions in Scheme 3 represent the typical one-electron oxidations of **2**, which are common to iron porphyrin chemistry. The purpose of the oxidation of **2** with $PhICl_2$ was to generate a functionalizable iron(III) complex, **10**, which can be used as a starting material in coordination and organometallic chemistry of iron(III). Complex **10** contains a typical

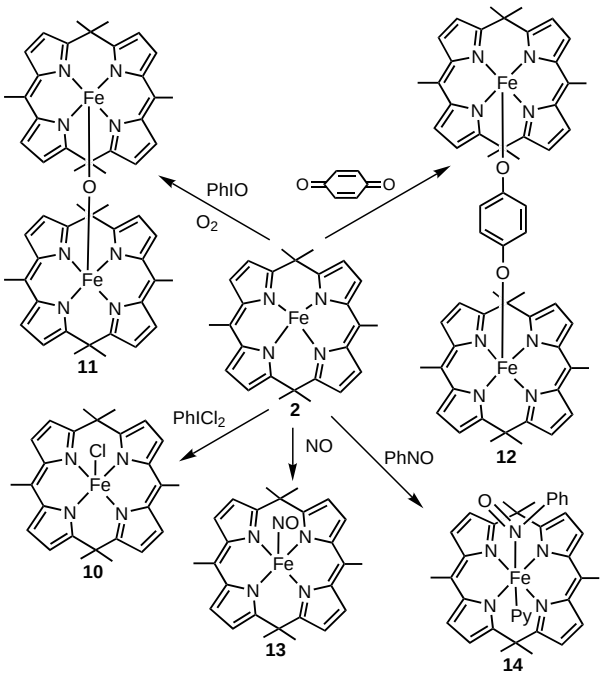


Scheme 3. The one-electron oxidation of hexaethylporphodimetheneiron(II) (**2**).

high-spin iron(III) ion ($\mu_{eff} = 5.55\,\mu_B$) in a five-coordinate environment. The reaction of **2** with dioxygen as an oxo-transfer agent led to the formation of the $\mu$-oxo derivative, **11**. *p*-Benzoquinone was used as a two-electron oxidizing agent, mimicking the conversion of dioxygen into a peroxo dianion, which is not followed by any O–O bond cleavage. The two related reactions with NO and nitrosobenzene have similar features. A solution of **2** in benzene exposed to NO gave dark red crystals of **13**, displaying a $\nu_{NO}$ stretching frequency at 1690.6 $cm^{-1}$. Any attempt to convert it into a hexacoordinated complex by the use of σ-binding ligand, such as pyridine, failed. Nitrosobenzene has often been used as an oxo-transfer agent in combination with iron(II) complexes. The preliminary coordination of PhNO has been found to preceed the deoxygenation reaction. Complex **14**, formed from a solution of **2** in benzene and PhNO in the presence of pyridine, did not show any change upon heating, and can be considered a structural model for the first stage of the nitrosobenzene deoxygenation reaction.

**Structural studies**: $^1H$ NMR spectroscopy is a useful analytical tool for inspecting the structure of the diamagnetic porphodimetheneiron(II) complexes in solution. All complexes, namely **4**, **6**, **7**, and **9**, have a two-fold symmetry that gives rise to a couple of doublets for the pyrrole $\beta$-hydrogens. The two ethyl groups in the monosubstituted *meso* positions are equivalent, as are the four ethyls in the two disubstituted *meso* positions, as expected for $D_{2h}$ symmtery, while three different kinds of ethyl groups are visible in the $C_{2v}$ symetric complexes.

The the solid-state structures will be analyzed according to the two most influential parameters, namely the coordination number of the metal and its oxidation state. The parent compound **2**, containing a tetracoordinated iron in a quasi-planar geometry, can add either one or two ligands in the axial positions and can undergo one-electron oxidation. The two above-mentioned parameters greatly affect the conformation of the ligand and, by consequence, the ligand-to-metal bonding.

The solid-state structural analysis will examine three classes of compounds: the parent complex **2**; the hexacoordinate iron compounds **6**, **7**, **9**, and **14**; and the pentacoordinate iron derivatives **8**, **10**, **11**, and **13**. The criterion adopted here for comparison is the coordination number rather than the oxidation state of the metal. Crystal data are listed in Table 1, conformational parameters in Table 2, and selected bond lengths and angles in Table 3.

Complex **2** (Figure 1) shows a nearly planar environment for the iron(II) metal ion. The small distortion observed within the coordination plane (out-of-plane $Fe\cdots N_4 = -0.045(1)$ Å, $N4–Fe1–N2 = 177.5(1)^\circ$, $N3–Fe1–N1 = 177.2(1)^\circ$) are mostly due to the conformation of the ligand (Table 2). The Fe–N bond lengths vary in a narrow range (1.949(2) – 1.954(2) Å) and are significantly shorter than those in the related iron(II) porphyrin compounds.[8] Such a shortening of the Fe–N distances is probably due to the highly distorted conformation of the ligand, which shows a really pronounced roof conformation (Table 2) with a high degree of ruffling along the *meso* $sp^2$ carbon atoms. The iron center is sterically protected in the axial positions by the hydrogen from the ethyl groups of the same or adjacent units. The intramolecular Fe–H interaction with a methylenic group occurs at 3.07 Å, while the methyl of an adjacent molecule approaches the metal with a Fe–H distance of 2.91 Å.

The hexacoordinate complexes **7**, **9**, and **14** (Figures 2 – 4) have similar structural features that can be summarized as follows: a) low-spin state, b) small displacement of the metal ion from the least-square $N_4$ plane ($-0.090(7)$ Å in **6**, 0.00 Å in **7**, 0.070(1) Å in **9**, and $-0.112(2)$ Å in **14**), c) slight distortion of the ideal octahedral coordination geometry, and d) the Fe–N average distances are in relatively good agreement (except for complex **7**) with those found in similar six-coordinate iron porphyrin derivatives (1.98(1) Å in **6**, 2.042(3) Å in **7**, 1.976(2) Å in **9**, 1.992(4) Å in **14**). These values are slightly shorter than those of the corresponding iron porphyrin compounds, mostly because of the conformation of the ligand, which adopts the roof conformation with different degrees of ruffling around the *meso* $sp^2$ carbon atoms (except complex **7**). In complex **6** all bond lengths within the coordination sphere of the metal center (Fe–C = 1.77(2) Å and Fe–N(py) = 2.07(1) Å) are comparable with analogous compounds.[9] Compound **7** deserves a more detailed discussion. The iron isocyanide functionalities usually have an Fe–C bond length[9c] similar to those of porphyrin derivatives.[10] The bond angles involving the C–N moiety (171.6(3)° and



0947-6539/00/0624-4520 $ 17.50+.50/0 *Chem. Eur. J.* **2000**, *6*, No. 24

Table 1. Crystal data and details of the structure determination for **2**, **7**–**9**, **11**, **13**, and **14**.

| | **2** | **7** | **8** | **9** | **11** | **13** | **14** |
|---|---|---|---|---|---|---|---|
| formula | $C_{32}H_{38}FeN_4$ | $C_{42}H_{56}FeN_6$ | $C_{33}H_{38}FeN_5$ | $C_{38}H_{43}FeN_6$ | $C_{64}H_{76}Fe_2N_8O$ | $C_{32}H_{38}FeN_5O$ | $C_{43}H_{48}FeN_6O$ |
| $M_w$ | 534.51 | 700.78 | 802.99 | 961.19 | 1085.03 | 564.52 | 720.72 |
| crystal system | monoclinic | triclinic | monoclinic | monoclinic | monoclinic | monoclinic | orthorhombic |
| space group | $P2_1/n$ | $P\bar{1}$ | $P2_1/n$ | $P2_1/n$ | $P2_1/n$ | $P2_1/n$ | $Pna2_1$ |
| $a$ [Å] | 8.7320(17) | 9.0900(18) | 11.492(2) | 11.910(2) | 11.892(2) | 12.593(3) | 15.8161(15) |
| $b$ [Å] | 13.241(3) | 11.024(2) | 20.379(3) | 32.733(7) | 20.000(4) | 13.847(3) | 17.6988(13) |
| $c$ [Å] | 23.242(5) | 11.545(2) | 19.787(4) | 14.779(3) | 23.823(5) | 16.686(3) | 13.1359(11) |
| $\alpha$ [°] | 90 | 68.07(3) | 90 | 90 | 90 | 90 | 90 |
| $\beta$ [°] | 100.71(2) | 67.25(3) | 101.33(3) | 108.76(3) | 99.03(3) | 109.70(3) | 90 |
| $\gamma$ [°] | 90 | 66.70(3) | 90 | 90 | 90 | 90 | 90 |
| $V$ [Å$^3$] | 2640.4(9) | 946.1(3) | 4543.7(14) | 5455.4(19) | 5595.8(19) | 2739.3(9) | 3677.1(5) |
| $Z$ | 4 | 1 | 4 | 4 | 4 | 4 | 4 |
| $\rho_{calcd}$ [g cm$^{-3}$] | 1.345 | 1.230 | 1.174 | 1.170 | 1.288 | 1.369 | 1.302 |
| $F(000)$ | 1136 | 376 | 1744 | 2080 | 2304 | 1196 | 1528 |
| $\mu$ [mm$^{-1}$] | 0.600 | 0.436 | 0.371 | 0.321 | 0.568 | 0.586 | 0.453 |
| $\lambda$ [Å] | 0.71070 | 0.71070 | 0.71070 | 0.71070 | 0.71070 | 0.71070 | 0.71073 |
| measured reflections | 14819 | 4252 | 25222 | 26012 | 26340 | 13397 | 21478 |
| unique reflections | 4495 | 2565 | 7391 | 7797 | 8387 | 4351 | 6069 |
| observed reflections [$I > 2\sigma(I)$] | 3586 | 2260 | 5870 | 5426 | 4973 | 2775 | 5780 |
| data/parameters | 4495/335 | 2565/224 | 7391/506 | 7797/633 | 8387/677 | 4351/353 | 6069/461 |
| $R$[a] [$I > 2\sigma(I)$] | 0.0383 | 0.0550 | 0.0478 | 0.0499 | 0.0495 | 0.0435 | 0.0626 |
| $wR2$[a] (all data) | 0.1114 | 0.1522 | 0.1436 | 0.1412 | 0.1315 | 0.1086 | 0.1593 |
| GoF[b] | 1.037 | 1.139 | 1.077 | 1.003 | 0.878 | 0.928 | 1.067 |

[a] $R = \Sigma||F_o| - |F_c||/\Sigma|F_o|$, $wR2 = \{\Sigma[w(F_o^2 - F_c^2)^2]/\Sigma[w(F_o^2)^2]\}^{1/2}$. [b] GoF $= \{\Sigma[w(F_o^2 - F_c^2)^2]/(n-p)\}^{1/2}$ in which $n$ is the number of data and $p$ is the number of parameters refined.

Table 2. Comparison of relevant structural parameters within the metal–ligand units in compounds **2**, **7**–**9**, **11**, **13**, and **14**.

| | | **2** | **7** | **8** | **9** | **11**[b] | | **13** | **14** |
|---|---|---|---|---|---|---|---|---|---|
| deviations from | N1 | 0.003(1) | 0 | −0.023(1) | −0.007(1) | −0.015(1) | [0.001(1)] | 0.004(1) | −0.028(2) |
| the $N_4$ core [Å] | N2 | −0.003(1) | 0 | 0.023(1) | 0.007(1) | 0.015(1) | [−0.001(1)] | −0.004(1) | 0.028(2) |
| | N3 | 0.003(1) | 0 | −0.023(1) | −0.007(1) | −0.015(1) | [0.001(1)] | 0.004(1) | −0.028(2) |
| | N4 | −0.003(1) | 0 | 0.023(1) | 0.007(1) | 0.015(1) | [−0.001(1)] | −0.004(1) | 0.028(2) |
| | Fe1 | −0.045(1) | 0 | 0.507(1) | 0.070(1) | 0.514(2) | [−0.509(2)] | −0.256(1) | −0.112(2) |
| angle between AB[a] [°] | | 23.2(1) | 4.8(1) | 8.8(2) | 17.7(1) | 22.4(2) | [21.8(2)] | 21.7(1) | 19.5(2) |
| angle between AC[a] [°] | | 48.7(1) | 0 | 38.8(1) | 45.3(1) | 35.9(2) | [31.2(2)] | 45.3(1) | 41.7(2) |
| angle between AD[a] [°] | | 41.7(1) | 4.8(1) | 30.3(1) | 36.1(1) | 26.9(2) | [21.1(2)] | 45.3(1) | 42.7(2) |
| angle between BC[a] [°] | | 39.1(1) | 4.8(1) | 32.0(1) | 43.3(1) | 25.3(2) | [21.9(2)] | 32.1(1) | 39.5(3) |
| angle between BD[a] [°] | | 46.5(1) | 0 | 23.4(1) | 41.1(1) | 34.9(2) | [30.6(2)] | 44.5(1) | 49.0(2) |
| angle between CD[a] [°] | | 25.2(1) | 4.8(1) | 8.7(2) | 16.3(1) | 24.7(2) | [22.2(2)] | 24.3(1) | 18.4(3) |
| angle between *meso* C $sp^2$ moieties [°] | | 53.1(1) | 0 | 34.3(1) | 54.0(1) | 30.7(2) | [23.7(3)] | 35.5(1) | 48.0(3) |

[a] A, B, C and D define the pyrrole rings containing N1, N2, N3, and N4. [b] The values in brackets refer to the second metal–ligand unit: Fe2, N5, N6, N7, and N8.

Table 3. Selected bond lengths [Å] and angles [°] for compounds **2**, **7**–**9**, **11**, **13**, and **14**.

| | **2** | **7**[a] | **8** | **9** | **11**[b] | | **13** | **14** |
|---|---|---|---|---|---|---|---|---|
| Fe–N1 | 1.954(2) | 2.042(3) | 2.119(2) | 1.984(2) | 2.067(3) | [2.071(3)] | 1.962(2) | 1.994(4) |
| Fe–N2 | 1.953(2) | 2.042(3) | 2.134(2) | 1.966(2) | 2.069(3) | [2.080(3)] | 1.954(2) | 1.995(4) |
| Fe–N3 | 1.949(2) | 2.042(3) | 2.109(2) | 1.984(2) | 2.068(3) | [2.078(3)] | 1.970(2) | 1.984(4) |
| Fe–N4 | 1.952(2) | 2.042(3) | 2.121(2) | 1.968(2) | 2.068(3) | [2.071(3)] | 1.983(2) | 1.994(4) |
| Fe–C[c] | | 1.907(4) | 2.091(3) | 1.922(3) | | | | |
| C–N[c] | | 1.168(5) | 1.153(3) | 1.172(3) | | | | |
| Fe–N(py)[c] | | | 2.091(3) | 2.061(2) | | | | 2.116(4) |
| Fe-C-N[c] | | 171.6(3) | 178.3(2) | 179.4(2) | | | | |
| Fe–O[c] | | | | | 1.762(2) | [1.770(2)] | | |
| Fe-O-Fe[c] | | | | | 178.6(2) | | | |
| Fe–N[c] | | | | | | | 1.708(2) | 1.839(4) |
| N–O[c] | | | | | | | 1.172(3) | 1.275(4) |
| Fe-N-O[c] | | | | | | | 147.3(2) | 117.8(3) |

[a] In the case of complex **7**, N3 and N4 correspond to N1′ and N2′ obtained by the following symmetry operations: $-x, -y, -z$. [b] Values in brackets correspond to the second metal–ligand unit. [c] Geometrical parameters which refer to the different axial ligands.

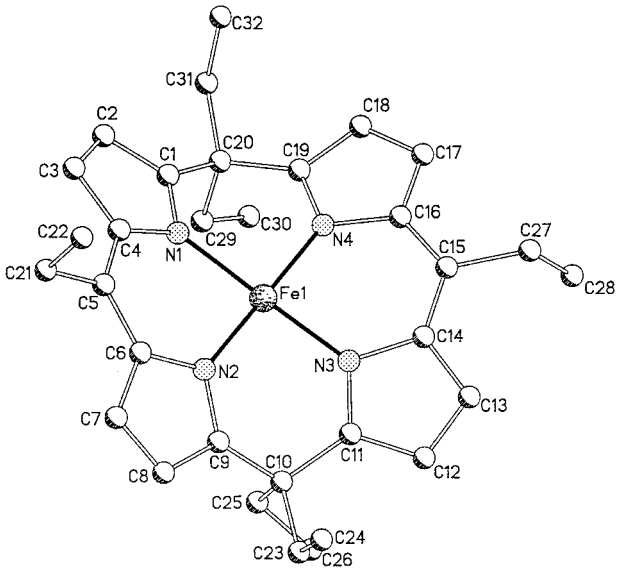


Figure 1. Ball-and-stick representation of complex **2** showing the adopted labeling scheme (hydrogens omitted for clarity).

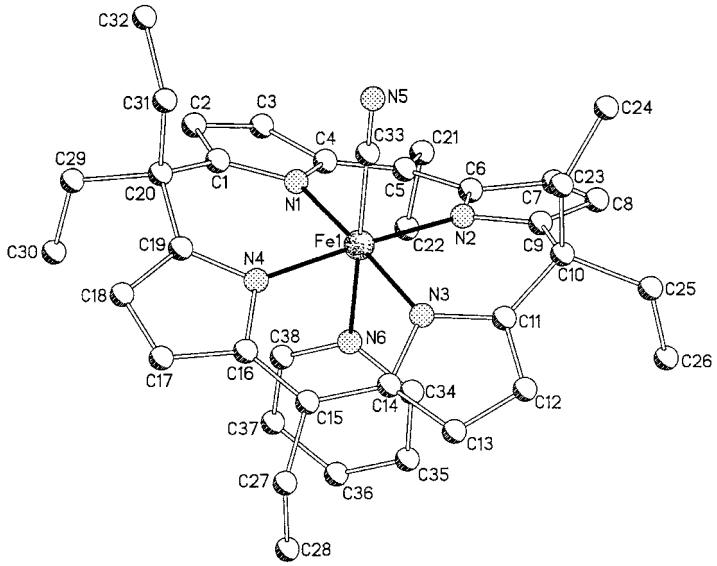


Figure 3. Ball-and-stick representation of the anion of complex **9** showing the adopted labeling scheme (hydrogens, $N(t\mathrm{Bu})_4^+$ cation, and solvent molecule omitted for clarity).

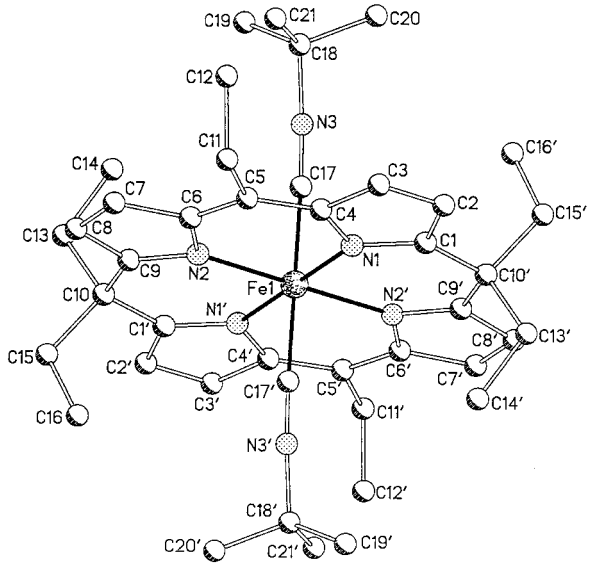


Figure 2. Ball-and-stick representation of complex **7** showing the adopted labeling scheme (hydrogens omitted for clarity). Prime denotes the following symmetry operation: $-x, -y, -z$.

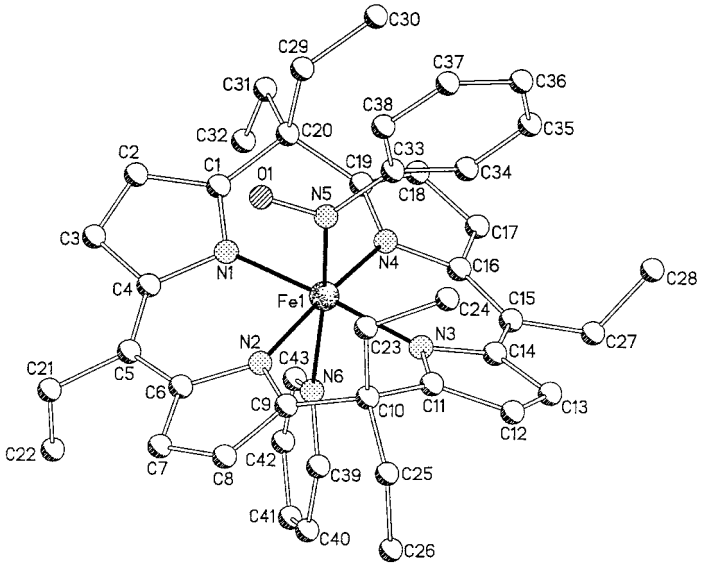


Figure 4. Ball-and-stick representation of complex **15** showing the adopted labeling scheme (hydrogens omitted for clarity).

169.4(3)°) show significant deviations from linearity as a consequence of the crystal packing. The lengthening of the Fe–N (2.042(3) Å) bond lengths by approximately 0.04 Å relative to those of the porphyrin analogues is due to the ligand thathas a larger $N_4$ cavity, when assuming a planar conformation. In the latter case, the larger size of the cavity is determined by the presence of two *meso* $sp^3$ carbons. In fact the distance between the two *meso* $sp^2$ carbon atoms (C–C = 6.889(5) Å) is similar to that found in planar porphyrins, whereas the distance between the two meso $sp^3$ carbon atoms (C–C = 7.181(5) Å) is about 0.3 Å longer. The ligand is almost planar (Table 2) with a small ruffling around the *meso* ($sp^3$ and $sp^2$) carbon atoms by 4.8(1)°. In complex **9**, bond lengths within the coordination sphere of the metal ion are in good agreement with those in related porphyrin compounds,[11] while the Fe–C bond length is 1.922(3) Å and that of Fe1–N(py) is 2.061(2) Å. In complex **14**, the Fe1–N5 and N5–O1 bond lengths (1.839(4) and 1.275(4) Å, respectively) are longer than those observed in complex **13**. The mutual disposition of the FeNO and Ph moieties is shown by the angles between the two planes (15.8(2)°) and by the following torsion angles: O1–N5–C33–C34, −164.8(4)°; O1–N5–C33–C38, 14.3(6)°. These values verify the steric effect that affects O1 and the hydrogen linked to C38. The comparison of the structural parameters of **14** with those of the PhNO derivatives of iron(II) porphyrins[12] shows that all the $Fe^{II}$–N bonds are in good agreement and that, in our case, an electronic π delocalization between N–O and the phenyl substituent is present, despite the above-mentioned steric effect. The metal ion completes its coordination sphere with a pyridine molecule (Fe–N(Py), 2.116(4) Å).



0947-6539/00/0624-4522 $ 17.50+.50/0 *Chem. Eur. J.* **2000**, *6*, No. 24

Complexes **8**, **11**, **13** (Figures 5–7), and **10** (Supporting Information), show very distorted square-pyramidal coordination geometry with significant deviation from the $N_4$ plane (0.507(1) Å in **8**, 0.462(5) Å in **10**, 0.514(2), −0.509(2) Å in **11**, and −0.256(1) Å in **13**). The Fe–N bond lengths are close to those observed in the five-coordinate iron porphyrin compounds bearing the same kind of axial ligand.[7, 9] They average to 2.121(2) Å in **8**, 2.066(9) Å in **10**, 2.068(3) and 2.075(3) Å in **11**, and 1.967(2) Å in **13**. The last value is typical for an iron(II) low-spin porphyrin, whereas those in the first three cases resemble iron(II) high-spin porphyrins, **8**, or high-spin iron(III) porphyrins, **10** and **11**. The ligand displays a very distorted roof conformation with different degrees of ruffling (Table 2). In complex **8** the Fe–C bond is very long (2.091(3) Å) and cannot be compared with the values reported for cyano hexacoordinate iron(II) porphyrins.[13] Such a long Fe–C bond is really unusual and is understandable on the basis of the lack of any back-donation from a high-spin iron(II). The Fe–Cl bond length (2.253(3) Å) in complex **10** is as expected for a high-spin iron(III).[14] The very short Fe1–O1 (1.762(2) Å) and Fe2–O1 (1.770(2) Å) bond lengths and the Fe–O–Fe (178.6(2)°) angle in complex **11**, which are close to those in the $\mu$-oxo iron(III) porphyrin,[15] support a quite strong Fe–O π-interaction. The two macrocycles are rotated by about 41° relative to each other, decreasing the steric hindrance between the ethyl groups. The distance between the ligands was estimated by using different parameters: the distance between the centroid of the pyrrolyl moieties and the *meso* carbon atoms that are just below or above them (3.985(3)–4.017(3) Å for $sp^2$ carbon atoms; 5.328(3)–5.417(3) Å for $sp^3$ carbon atoms), the distance (4.555(3) Å) and the angle (1.5(1)°) between the two planes defined by the core nitrogens (N1, N2, N3, N4, N5, N6, N7, N8), and the distance between the two metals (3.532(1) Å). Such values clearly indicate that the two ligands, though highly distorted in the usual "roof" fashion with a high degree of ruffling, are almost parallel and the rotation is mainly determined by hindrance between the peripheral substituents. The Fe1–N5 (1.708(2) Å) and N5–O1 (1.172(3) Å) bond lengths and the Fe–N–O bending (Fe1–N5–O1 = 147.3(2)°) in complex **13** are close to those in some nitrosyl iron porphyrins[16] and suggest a significant Fe–N π interaction and the reduction of the effective oxidation state of the metal. Moreover, complex **13** has a tilting Fe–N(NO) axis from the $N_4$ mean plane normal toward the mono-substituted *meso* carbon and the two Fe–$N_p$ bond lengths along the Fe–NO bond-tilt direction are shortened with respect to the two Fe–$N_p$ distances in the other direction. It is worth noting that these features are very close to those recently observed in two high-quality X-ray

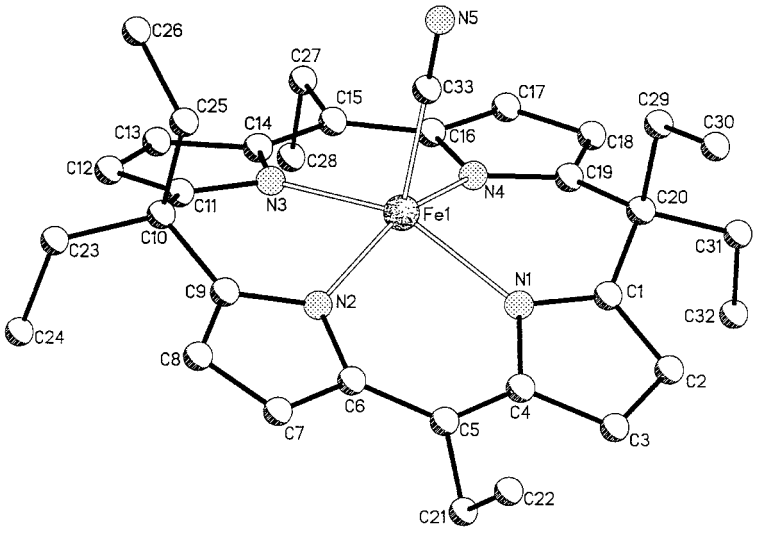


Figure 5. Ball-and-stick representation of the anion of complex **8** showing the adopted labeling scheme (hydrogens and $N(tBu)_4^+$ cation omitted for clarity).

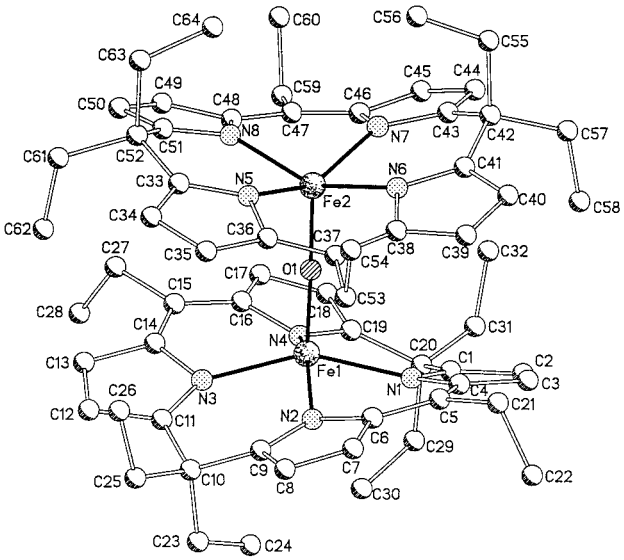


Figure 6. Ball-and-stick representation of complex **11** showing the adopted labeling scheme (hydrogens omitted for clarity).

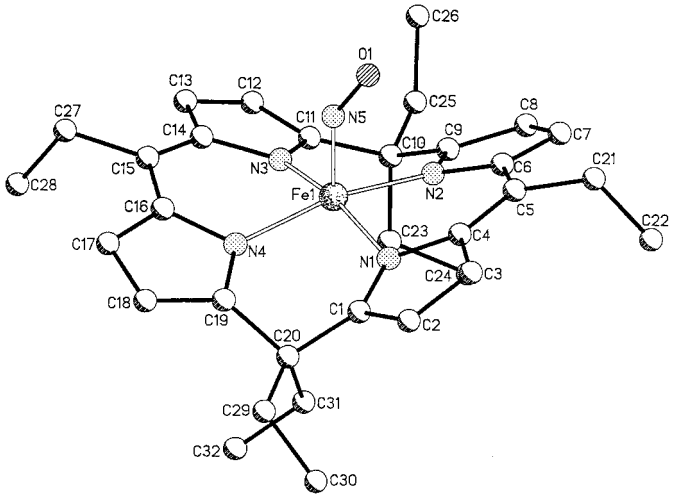


Figure 7. Ball-and-stick representation of complex **13** showing the adopted labeling scheme (hydrogens omitted for clarity).

structures of [Fe(OEP)(NO)] (OEP = octaethylporphyrin).[17]

Historically, the analytical tool most often employed for identifying porphyrin modifications has been UV/Vis spectroscopy. All of our iron(II) and iron(III) complexes have been examined with this technique. Iron(II) complexes have an intense absorption maximum between 440 and 460 nm with a second weak band around 500 nm (Figure 8a). The second peak is slightly red-shifted by 20–30 nm passing from low-spin hexacoordinate to high-spin hexacoordinate and high-spin pentacoordinate complexes and is decreased to a shoulder in the intermediate-spin tetracoordinated complex **2**. These absorption bands are similar to those observed for other metallodiporphomethenes[3h, 18] and probably originate from $\pi-\pi^*$ ligand transitions. The electronic absorption spectra of the iron(II) porphodimethenes somewhat resemble those of iron(II) porphyrins, which are characterized by an intense transition at 400–420 nm (the Soret or B band) and a pair of vibrationally resolved weak transitions at 550–600 nm (the Q bands). These have been assigned to single excitations from $a_{1u}$, $a_{2u}$ porphyrin $\pi$ orbitals to $e_g^*$ porphyrin $\pi^*$ orbitals, to form four excited states that can mix by configuration interaction.[19] In the iron porphodimethenes, however, the Soret band is replaced by a characteristic "methene" band, which is at lower energy and has a smaller extinction coefficient.

Iron(III) complexes show more complicated spectra, characterized by three bands, two intense ones in the 360–390 nm and 440–460 nm regions and a weaker one at 480–520 nm. A few other weak bands are also observed around and above 600 nm and are probably due to charge transfer and/or d–d transitions (Figure 8b). Such spectra are similar to those observed for iron(III) decaalkylporphodimethenes,[20] which also show a split of the methene band. The iron(III) porphodimethene spectra present some analogies with the spectrum of [(TPP)FeCl] (TPP = tetraphenylporphyrin), which, in addition to the B and Q bands, display a third relatively intense band around 380 nm;[19, 21] again, no Soret band is observed.

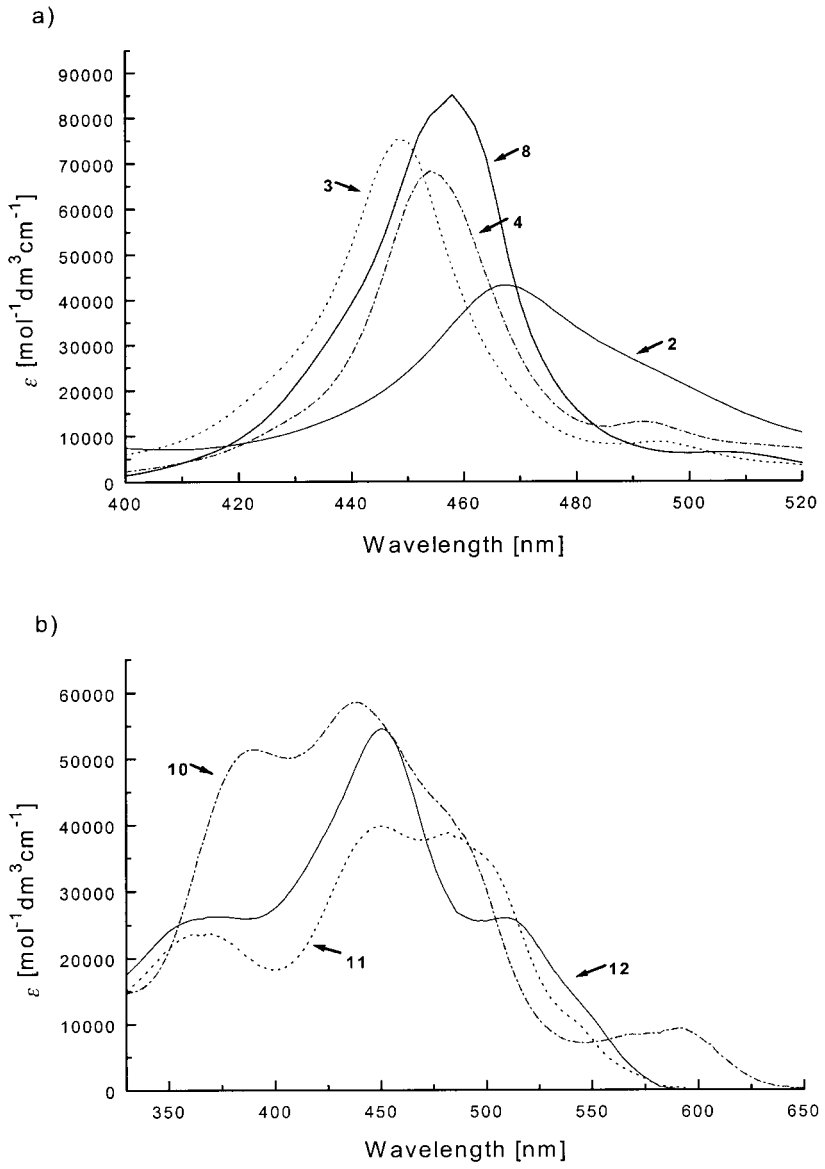


Figure 8. The UV/Vis spectra of a) **2**, **3**, **4**, and **8**; and b) **10**–**12**.

**Magnetic studies**: The magnetic susceptibilities of complexes **2**, **3**, **8**, and **10**–**13** were collected in the temperature range of 1.9–300 K, and those of **2**, **3**, **8**, and **11**–**12** are shown in Figures 9–11.

*Iron(II) complexes*: The $d^6$ $Fe^{II}$ ion can exhibit three spin states, the $S=0$ low-spin state, the $S=1$ intermediate-spin state and the $S=2$ high-spin state. Although the intermediate spin cannot be observed in an ideal octahedral environment, it has been observed for some severely distorted tetragonal or pyramidal coordination environments(see below).

The temperature dependence of the magnetic moments of **2** is illustrated in Figure 9. The magnetic moment is almost constant between 300 and 80 K, with a room-temperature value of 3.65 $\mu_B$, and shows a sudden decrease below 80 K, reaching 0.85 $\mu_B$ at 2 K. The room-temperature value of the effective magnetic moment is consistent with an $S=1$ intermediate-spin state, while the decrease at low temperature can be attributed to a large zero-field splitting with a nonmagnetic level lying lowest. This behavior is quite similar to that of other tetracoordinated $Fe^{II}$ complexes



0947-6539/00/0624-4524 $ 17.50+.50/0 *Chem. Eur. J.* **2000**, *6*, No. 24

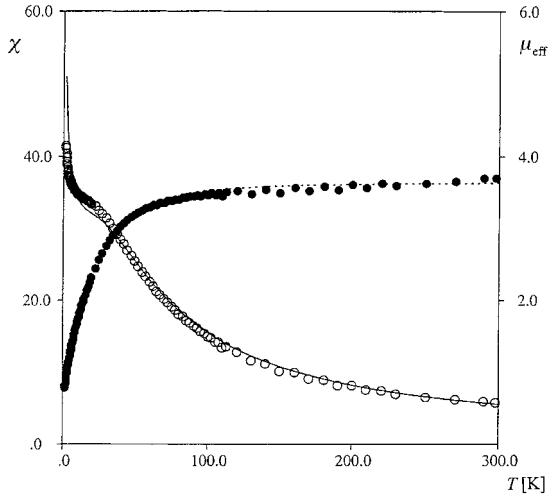


Figure 9. Magnetic susceptibilities (○) [$10^{-3}$ emu] and magnetic moments (●) [$\mu_B$] as a function of the temperature for complex **2**.

with square-planar coordination of an $N_4$ macrocyclic ligand.[22, 23] The room-temperature magnetic moment of **2** is very close to that reported for [Fe(Pc)] (Pc = phtalocyanine), $\mu_{eff} = 3.9\,\mu_B$,[22] and slightly lower than that of [Fe(TPP)] (TPP = tetraphenylporphyrin), $\mu_{eff} = 4.2\,\mu_B$.[23] The magnetic data have been analyzed in terms of an isolated $S = 1$ state with an isotropic g-factor and an axial zero-field splitting described by the following spin hamiltonian:[24] $\hat{\boldsymbol{H}} = \mu_B g \boldsymbol{H} \cdot \boldsymbol{S} + D[\boldsymbol{S}_z^2 - S(S+1)/3]$, in which $S = 1$ and $D$ is the zero-field-splitting constant. The spin degeneracy of the $S = 1$ state is partly lifted by spin-orbit coupling into the $M_s = 0$ and $M_s = \pm 1$ components, separated by the zero-field-splitting parameter $D$. The magnetic susceptibility can be derived by using the Van Vleck equation and is given by Equation (1), with $x = D/kT$.[24a] A good fit was found for g = 2.56 and D = 74.8 $cm^{-1}$ (see solid line in Figure 9).

$$\chi = \frac{Ng^2\mu_B^2}{3kT}\,\frac{\exp(-x) + (2/x)[1 - \exp(x)]}{1 + 2\exp(-x)} \qquad (1)$$

The coordination of one or two axial ligands to **2** drastically changes its magnetic behavior. A summary of the magnetic properties of polycrystalline samples of the characterized [Fe($Et_6N_4$)(L)(L′)] complexes is given in Table 4. We see that most of these compounds are diamagnetic (**4**–**7**, **9**, and **14**) and that only the pentacoordinate cyanide complex **8** and the hexacoordinate THF complex **3** show a high-spin ground state. Indeed, the temperature dependence of the magnetic moments of **3** and **8** (Figure 10) is typical of a high-spin $Fe^{II}$ $d^6$ monomer ($S = 2$), the magnetic moment being constant in almost the whole temperature range 2–300 K, with values of 5.35 $\mu_B$ and 4.72 $\mu_B$, respectively, at 298 K.

Table 4. Summary of the magnetic properties of complexes **2**–**9**, **13**, and **14** {[Fe($Et_6N_4$)(L)(L′)]}.

| | L | L′ | $\mu_{eff}$ [298 K] | $\mu_{eff}$ [2 K] | Spin state | Features |
|---|---|---|---|---|---|---|
| **2** | none | none | 3.65 | 0.85 | 1 | intermediate spin |
| **3** | THF | THF | 5.35 | 4.10 | 2 | high Spin |
| **4** | Py | Py | – | – | 0 | diamagnetic |
| **5** | CO | CO | – | – | 0 | diamagnetic |
| **6** | CO | Py | – | – | 0 | diamagnetic |
| **7** | CN*t*Bu | CN*t*Bu | – | – | 0 | diamagnetic |
| **8** | $CN^-$ | none | 4.72 | 2.90 | 2 | high Spin |
| **9** | $CN^-$ | Py | – | – | 0 | diamagnetic |
| **13** | NO | none | 1.85 | 1.80 | 1/2 | low spin {FeNO}[7] |
| **14** | PhNO | Py | – | – | 0 | diamagnetic |

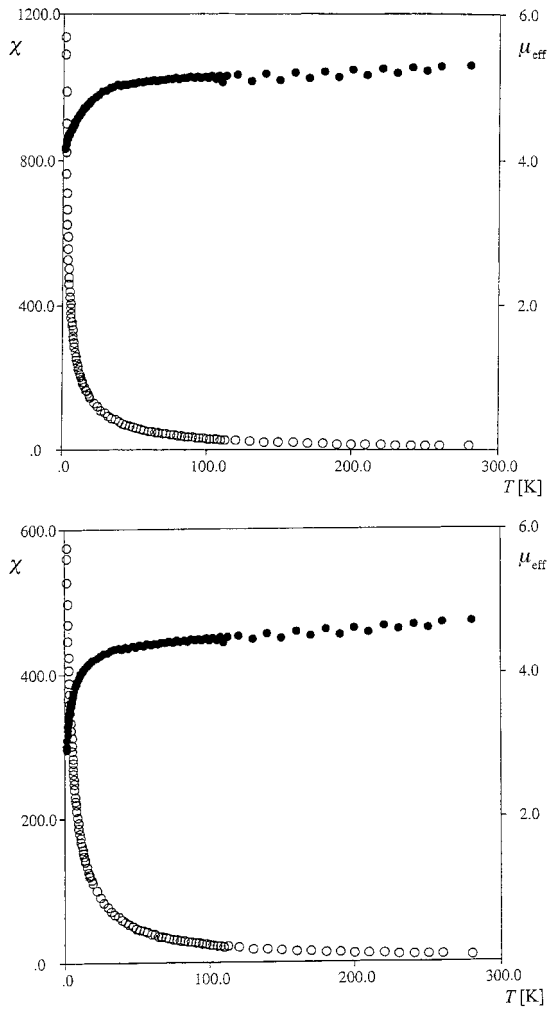


Figure 10. Magnetic susceptibilities (○) [$10^{-3}$ emu] and magnetic moments (●) [$\mu_B$] as a function of the temperature for complexes **3** (top) and **8** (bottom).

It is interesting to compare the magnetic behavior of these four-, five-, and six-coordinate iron(II) porphodimethene complexes with the related iron(II) porphyrin complexes whose structural and electronic features have been probed in considerable depth in the past.[7b, 25, 26]

For porphyrin complexes the spin state of the iron(II) center is determined by the nature and the number of axial ligands: the coordination of strong-field ligands (Py, CO, etc.) leads to low-spin, six-coordinate complexes, while the coordination of weaker field ligands (THF, 2-MeIm, RS-, etc.) leads to high-spin, five- or six-coordinate complexes; the absence of any axial ligands leads to an intermediate-spin complex. Therefore, the decrease of the axial ligand field gives sequentially low-spin, high-spin, and intermediate-spin states. These observations have been interpreted in terms of ligand-field effects on the d-orbital splitting,[25, 26] which for an iron

porphyrin is given by three nearly degenerate low-lying $d_{xy}$, $d_{xz}$, $d_{yz}$ orbitals, the high-lying $d_{x^2-y^2}$ orbital, whose lobes point towards the porphyrinato nitrogen atoms, and the $d_{z^2}$ orbital, whose energy is strongly affected by the axial ligand field. In particular the high energy of the $d_{x^2-y^2}$ orbital destabilizes the high-spin state, while the strong dependence of the $d_{z^2}$ orbital on the axial ligand field may determine a low-, intermediate-, or high-spin ground state.

Essentially the same spin-state/stereochemical relationships also apply for the iron(II) porphodimethene complexes addressed in this work. Indeed, although porphodimethene has a slightly larger macrocycle coordination cavity (as a consequence of two *meso* $sp^3$ carbons), it is also more flexible and can better adapt to the smaller low- or intermediate-spin iron(II) radius through combined rooflike and ruffling deformations.

The magnetic moment of **13** is constant in the whole range of temperatures with a value of 1.85 $\mu_B$ at 298 K, and clearly indicates an $S = 1/2$ low-spin state for this {FeNO}$^7$ species. Note that this is the same behavior observed for iron(II) porphyrin five-coordinate nitrosyl derivatives.[28]

*Iron(III) complexes*: The temperature dependence of the magnetic moment of **10** is typical of a high-spin $Fe^{II}$ $d^5$ monomer ($S = 5/2$), the magnetic moment being constant in the temperature range 30–300 K with a value of 5.85 $\mu_B$ at 298 K, and decreasing below 30 K because of zero-field splitting.

The temperature dependence of the magnetic moments of **11** and **12** shows a steady decrease from 300 to 1.9 K (Figure 11) and is typical of antiferromagnetic coupled $Fe^{III}$ dinuclear compounds. The data were fitted with the theoretical equation [Eq. (2)], in which $x = 2J/kT$[24] based on the Heisenberg model $\hat{\boldsymbol{H}} = -2J\hat{\boldsymbol{S}}_1\hat{\boldsymbol{S}}_2$ ($S_1 = S_2 = 5/2$).

$$\chi_{dim} = \frac{Ng^2\mu_B^2}{kT}\,\frac{\exp(x) + 5\exp(3x) + 14\exp(6x) + 30\exp(10x) + 55\exp(15x)}{1 + 3\exp(x) + 5\exp(3x) + 7\exp(6x) + 9\exp(10x) + 11\exp(15x)} \quad (2)$$

To obtain a good fit we included a correction for a small number of mononuclear $Fe^{III}$ impurities, which were assumed to obey the Curie law. The following equation [Eq. (3)] is therefore used for the total susceptibility, where $S = 5/2$, $g'$ is the g-factor of the impurity (assumed 2.00), and $p$ is the mononuclear impurity fraction. The calculated best fit parameters are $g = 1.95$, $J = -115\ cm^{-1}$, $p = 4.6\,\%$ for **11**, and $g = 1.82$, $J = -9.4\ cm^{-1}$, $p = 3.9\,\%$ for **12**.

$$\chi = 1/2(1-p)\chi dim + p\,\frac{Ng'^2\mu_B^2 S(S+1)}{3kT} \quad (3)$$

The $\mu$-oxo dinuclear complex **11** has a high Heisenberg coupling constant, $J = -115\ cm^{-1}$, slightly lower than the values reported for the analogous iron porphyrin $\mu$-oxo complexes, which range from $-120$ to $-145\ cm^{-1}$,[25, 29] and close to the value reported for the only previously characterized $\mu$-oxo porphodimethene iron(III) complex, $\mu$-oxo-bis[*meso*-dimethyloctaethylporphodimethene-$Fe^{III}$] with $J = 105\ cm^{-1}$.[30]

**Theoretical analysis—density functional investigation**: Density functional theory (DFT) calculations were performed to gain a better understanding of the main electronic and magnetic properties of the iron(II) complexes supported by the porphodimethene ligand and to elucidate the spin-state/stereochemical relationship in iron(II) porphodimethene complex. DFT calculations including nonlocal correction to the exchange correlation potential have recently been shown to adequately describe the geometry and the energy ordering of the lowest spin states of metalloporphyrins.[31, 32]

We analyzed several low-lying electronic states of **2**, performing a full geometry optimization under $C_{2v}$ constraints for each of them. The calculated energies are reported in Table 5 and show a triplet $^3B_1(d_{z^2})^1(d_{xz})^1$ ground state with a

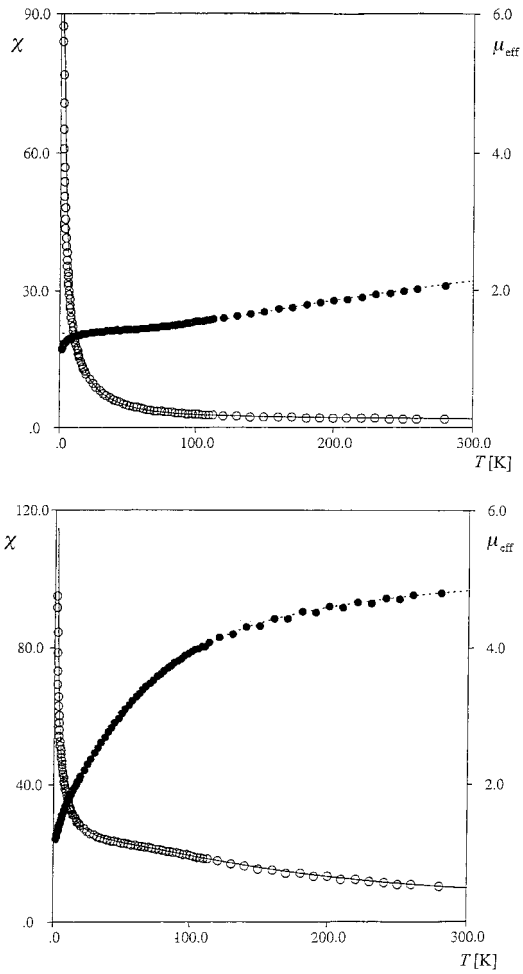


Figure 11. Magnetic susceptibilities (○) [$10^{-3}$ emu], and magnetic moments (●) [$\mu_B$] as a function of the temperature for complexes **11** (top) and **12** (bottom).

Table 5. Relative energies calculated for the lowest lying electronic states of **2**.

| State | Configuration | $\Delta E$ [eV] |
|---|---|---|
| $^1A_1$ | $(d_{x^2-y^2})^2(d_{z^2})^2(d_{xz})^2$ | 0.94 |
| $^3A_2$ | $(d_{x^2-y^2})^2(d_{z^2})^2(d_{xz})^1(d_{yz})^1$ | 0.06 |
| $^3A_1$ | $(d_{x^2-y^2})^1(d_{z^2})^1(d_{xz})^2(d_{yz})^2$ | 0.53 |
| $^3B_1$ | $(d_{x^2-y^2})^2(d_{z^2})^1(d_{xz})^1(d_{yz})^2$ | 0.00 |
| $^3B_2$ | $(d_{x^2-y^2})^2(d_{z^2})^1(d_{xz})^2(d_{yz})^1$ | 0.10 |
| $^5A_1$ | $(d_{x^2-y^2})^2(d_{z^2})^1(d_{xz})^1(d_{yz})^1(d_{xy})^1$ | 0.64 |
| $^5B_1$ | $(d_{x^2-y^2})^1(d_{z^2})^1(d_{xz})^2(d_{yz})^1(d_{xy})^1$ | 0.74 |
| $^5B_2$ | $(d_{x^2-y^2})^1(d_{z^2})^1(d_{xz})^1(d_{yz})^2(d_{xy})^1$ | 0.83 |



0947-6539/00/0624-4526 $ 17.50+.50/0 *Chem. Eur. J.* **2000**, *6*, No. 24

$^3A_2(d_{xz})^1(d_{yz})^1$ state only 0.06 eV higher in energy. Two more low-lying triplets lie within 0.6 eV of the ground state and three quintet states lie about 0.6–0.8 eV above the ground state. Table 6 reports the optimized geometries of the lowest electronic states of each spin symmetry; the numbering refers to the scheme given in Scheme 4.

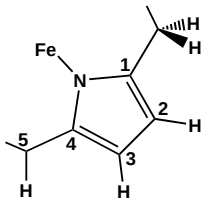


Scheme 4. Numbering scheme adopted for the porphyrinogen macrocycle.

The optimized geometry for the $^3B_1$ ground state is in fairly good agreement with the experimental X-ray data of **2** and reproduces the main structural features of metal porphodimethene, with a rooflike folding of the two halves of the macrocycle and a significant ruffling of the two pyrrolic rings within each half.

The experimental Fe–N core size (1.952 Å) is actually smaller than that calculated (2.008 Å) but this discrepancy could be due to the presence of the ethyl groups in the actual molecule, which would enhance the rooflike and ruffling distortions and lead to shorter Fe–N bonds. Indeed the out-of-plane ruffling of the porphyrin ring is known to shorten metal–N(porphyrin) bonds, as observed for the ruffled [Fe(TPP)] species, whose Fe–N bond length (1.972 Å)[8a] is significantly shorter than that for the planar [Fe(OEP)] (1.996 Å).[8b]

Table 6 also shows that the length of the Fe–N core is determined mainly by the electronic state and specifically by the occupancy of the antibonding $d_{x^2-y^2}$ orbital. In particular the core size is significantly larger for the quintet state (with occupied $d_{x^2-y^2}$) than for the triplet and singlet states; exactly the same behavior is observed for porphyrin complexes.[7b, 8, 25, 26]

Moreover, Table 6 shows an excellent agreement between the Fe–N bond and the other intraligand bond lengths calculated for the singlet and quintet states and the crystallographic results for the corresponding low- and high-spin six-coordinate iron(II) complexes **3** and **4**. This suggests that the axial ligands affect the metal porphodimethene geometry only through the determination of the spin state.

It is interesting to compare the electronic structure of the iron(II) porphodimethene complex with that of the iron(II) porphyrins, which have been the subject of several theoretical studies. In a recent paper, Spiro and co-workers reported the results of gradient corrected DFT calculations on the low-lying spin states of iron(II) porphyrin, indicating a $^3A_2$ $(d_{xz})^1(d_{yz})^1$ ground state (consistent with the majority of experimental evidence)[32] with a $^3E_g(d_{z^2})^1(d_{xz},d_{yz})^3$ very close in energy. This energy ordering is reversed in the iron(II) porphodimethene, whose ground state is the $^3B_1$ $(d_{z^2})^1(d_{yz})^1$ (with the same configuration of the iron porphyrin $^3E_g$ state), while the $^3A_2$ $(d_{xz})^1(d_{yz})^1$ is the first excited state. The vanishingly small energy difference between these two states (0.06 ev) makes the attribution of the ground state of **2** questionable.

In the attempt to investigate the reasons of this difference and to compare the electronic structure of the iron(II) porphodimethene and porphyrin complexes, we performed DFT calculations, at the same level of theory, on the $^3A_2$ ground state of iron(II) porphyrin. In Figure 12, we compare the main frontier orbitals for the two complexes obtained from spin-restricted calculations performed on the optimized geometries of the same $^3A_2$ state. The metal orbitals for the two complexes are quite similar, the main difference being the energy splitting of the degenerate $e_g(d_{xz},d_{yz})$ level of the iron

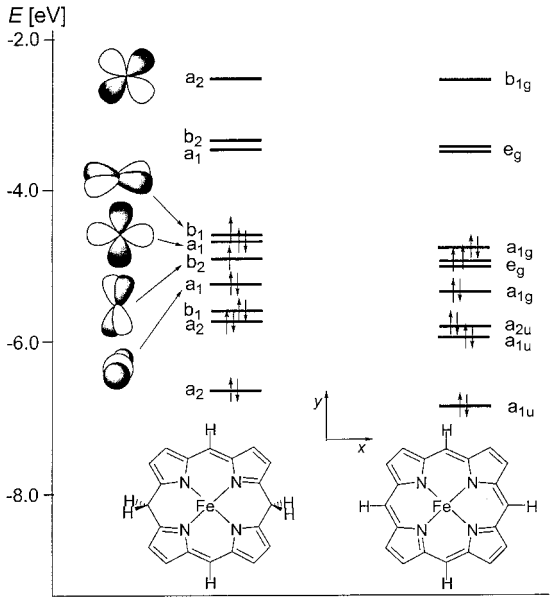


Figure 12. Molecular orbital diagram for iron(II) porphodimethene and porphyrin complexes in the $^3A_2$ state.

Table 6. Main geometrical parameters (bond lengths in Å) calculated for the three lowest states of each spin symmetry and their comparison with the experimental values. OOP is the out-of-plane deviation of Fe from the $N_4$ mean plane, $\varphi$ the angle between the two mean planes of the two porphodimethene halves, and $\theta$ is the ruffling angle between the pyrrole rings within one half.

| System | Fe–N | N–C1 | N–C4 | C1–C2 | C2–C3 | C3–C4 | C4–C5 | OOP | $\varphi$ | $\theta$ |
|---|---|---|---|---|---|---|---|---|---|---|
| theoretical | | | | | | | | | | |
| $^1A_1$ | 1.984 | 1.360 | 1.409 | 1.408 | 1.385 | 1.413 | 1.378 | 0.081 | 32.1 | 8.8 |
| $^3B_1$ | 2.008 | 1.351 | 1.401 | 1.415 | 1.380 | 1.418 | 1.384 | 0.079 | 32.2 | 7.4 |
| $^3A_2$ | 2.016 | 1.351 | 1.399 | 1.415 | 1.380 | 1.418 | 1.382 | 0.098 | 31.0 | 5.0 |
| $^5A_1$ | 2.094 | 1.346 | 1.395 | 1.419 | 1.383 | 1.422 | 1.391 | 0.181 | 31.1 | 6.1 |
| experimental | | | | | | | | | | |
| **4** | 1.980 | 1.349 | 1.408 | 1.425 | 1.361 | 1.424 | 1.392 | 0.043 | 51.8 | 17.4 |
| **2** | 1.952 | 1.355 | 1.397 | 1.417 | 1.365 | 1.419 | 1.389 | 0.045 | 53.1 | 24.2 |
| **3** | 2.098 | 1.342 | 1.406 | 1.422 | 1.361 | 1.423 | 1.400 | 0 | 0 | 2.7 |

  0947-6539/00/0624-4527 $ 17.50+.50/0 

porphyrin into $b_2$ and $a_1$ orbitals in the porphodimethene, with a significant stabilization of the $b_2(d_{yz})$ orbital which lies in the plane containing the two monosubstituted *meso* carbons. This splitting, although small, is probably responsible for the stabilization of the $^3B_1$ state in the porphodimethene complex.

Another important difference is the energy splitting of the lowest unoccupied $e_g^*$ orbital of iron porphyrin into the $b_2$ and $a_1$ in iron porphodimethene and the energy increase of the two highest porphodimethene $\pi$ orbitals, $a_1$ and $b_1$ (Figure 12). Since these two orbitals are involved in the $\pi-\pi^*$ transition that gives rise to the two main bands in the electronic absorption spectra of these complexes, these orbital changes are responsible of the observed differences between iron porphodimethene and iron porphyrin absorption spectra. Indeed the energy increase of the $\pi$ orbitals should lead to a red shift of the most intense B band, while the splitting of the $\pi^*$ orbitals should reduce the configuration interaction mixing of the two lowest excited states, thus decreasing the shift between B and Q bands and their intensities in agreement with experimental evidence (see above).

Density functional calculations were also performed on the nitrosyl derivative **13** by considering only the lowest doublet spin state $^2A'$. In the Enemark and Feltham notation this species has the same $\{FeNO\}^7$ electronic configuration of iron porphyrin nitrosyl complexes[28] and is therefore expected to have similar electronic and geometric structures. Five- or six-coordinate nitrosylmetalloporphyrin derivatives with $\{MNO\}^n$ configuration (where $n=6-8$) have been structurally and theoretically characterized.[28] The controlling factor in the bonding geometry is the number ($n$) of d electrons on the metal plus the unpaired electrons from NO. The M–N–O linkage is linear for $n=6$ and strongly bent (M–N–O$\approx 120^\circ$) for $n=8$, while complexes $n=7$ have intermediate M–N–O angles ($140-150^\circ$). This behavior was explained by Hoffman in terms of Walsh rule correlations on the bonding orbital that involves the metal $d_{z^2}$ and one of the $\pi^*$ orbitals of NO.[33] The crystallographic structure of **13** has a geometry of the FeNO group that is very close to that of iron(II) porphyrin nitrosyl complexes with a short Fe–N bond length (1.708 Å) and a bent Fe–N–O angle (147.3°) (Table 3).[17] When NO is bound to an iron porphodimethene unit, there are two possible limit conformations with the nitrosyl group bent/tilted along the $N_p$–Fe–$N_p$ bisectrices toward the monosubstituted or disubstituted *meso* carbons; however, only the former is observed in the solid-state structure. Two independent geometry optimizations in $C_s$ symmetry were performed for each of these two conformations, and that with the NO bent towards the monosubstituted *meso* carbon is energetically favored by about 1 kcal mol$^{-1}$, in agreement with the crystallographic structure. A geometry optimization in $C_{2v}$ symmetry was also performed on the complex with a linear Fe–N–O arrangement and showed that the energy required to bend the Fe–N–O angle from its equilibrium value (147.3°) to 180° is very small, only 3.5 kcal mol$^{-1}$. This value can be considered an upper limit for the energy barrier to rotation of the nitrosyl group around the Fe–N(NO) bond, so that this motion is expected to be essentially free above 200 K. The calculated main geometrical parameters are reported in Table 7 and are in good agreement with the X-ray data, reproducing, in particular, the tilting of the Fe–N(NO) axis, 4.6° versus 4.2°, and the asymmetry pattern of the Fe–$N_p$ bond lengths, 0.026 Å versus 0.021 Å.

Table 7. Main geometrical parameters (bond lengths in Å and angles in °) calculated for the nitrosyl complex **13**. The corresponding experimental values for **13** and [Fe(OEP)(NO)][7a] are also reported for comparison. $\chi$ is the angle between the Fe–N(NO) axis and the $N_4$ mean plane, Fe–$N_p{}^a$ and Fe–$N_p{}^b$ are the averages of the two Fe–$N_p$ bond lengths [Å] along the Fe–NO bond-tilt direction and of the two in the other direction, respectively, and $\Delta$ is their difference.

| | Fe–N | N–O | Fe-N-O | $\chi$ | Fe–$N_p{}^a$ | Fe-$N_p{}^b$ | $\Delta$ |
|---|---|---|---|---|---|---|---|
| theoretical | | | | | | | |
| $^2A'$ | 1.709 | 1.182 | 149.5 | 4.6 | 2.022 | 2.048 | 0.026 |
| experimental | | | | | | | |
| **13** | 1.708 | 1.172 | 147.0 | 4.2 | 1.958 | 1.979 | 0.021 |
| [Fe(OEP)(NO)] | 1.731 | 1.168 | 142.7 | 8.2 | 1.999 | 2.022 | 0.023 |

The analysis of the wave function for the lowest conformation shows that the spin density is localized mainly on the iron ion, although some residual spin density is also located on NO with a polarization opposite to that of iron. Indeed, the singly occupied molecular orbital consists essentially of the metal $d_{z^2}$ orbital with a minor contribution from the nitrosyl group. The $d_\pi$ orbitals of Fe are strongly mixed with the $\pi^*$ orbitals of NO, making questionable the assignment of formal oxidation state of the iron atom; however, the overall charge on the NO moiety ($-0.10$) suggests a prevalent $Fe^{III}-NO^-$ description.

## Experimental Section

**General**: All reactions were carried out under an atmosphere of purified nitrogen. Solvents were dried and distilled by standard methods before use. Infrared spectra were recorded with a Perkin–Elmer FT 1600 spectrophotometer. UV/Vis spectra were recorded with a Hewlett–Packard 8452A diode array spectrophotometer. NMR spectra were recorded on Bruker AC200E and DPX400 instruments. The synthesis of the ligand **1** was carried out according to the literature.[5] Magnetic susceptibility measurements were made on a MPMS5 SQUID susceptometer (Quantum Design) operating at a magnetic field strength of 1 kOe. Corrections were applied for diamagnetism calculated from Pascal constants.[34] Effective magnetic moments were calculated as $\mu_{eff}=2.828(\chi_{Fe}T)^{1/2}$ in which $\chi_{Fe}$ is the magnetic susceptibility per iron atom. Fitting of the magnetic data to the theoretical expression were performed by minimizing the agreement factor, defined as $\Sigma[\chi_i^{obsd}T_i-\chi_i^{calcd}T_i]^2/(\chi_i^{obsd}T_i)^2$, through a Levenberg–Marquardt routine.

**Computational and methodological details**: The calculations reported in this paper are based on the ADF (Amsterdam Density Functional) program package described elsewhere.[35] Its main characteristics are the use of a density-fitting procedure to obtain accurate Coulomb and exchange potentials in each self-consistent field (SCF) cycle, the accurate and efficient numerical integration of the effective one-electron hamiltonian matrix elements, and the possibility to freeze core orbitals. The molecular orbitals were expanded in an uncontracted triple-$\zeta$ Slater-type orbitals (STO) basis set for all main group atoms. For iron orbitals we used a double-$\zeta$ STO basis set for the 3s and 3p orbitals and a triple-$\zeta$ STO basis set for the 3d and 4s ones. As polarization functions, we used one 4p function for iron, one 3d for C and N, and a 2p function for H. The inner shell cores were kept frozen. The local density approximation (LDA) exchange correlation potential and energy were used, together with the Vosko–Wilk–Nusair parametrization[36] for homogeneous electron gas correlation, including the Becke's nonlocal correction[37] to the local exchange expression and the Perdew's nonlocal correction[38] to the local expression of correlation energy. Molecular structures of all considered complexes were optimized at this nonlocal (NL) level in $C_{2v}$ symmetry. The



0947-6539/00/0624-4528 $ 17.50+.50/0 *Chem. Eur. J.* **2000**, *6*, No. 24

iron(II) porphodimethene complex was only slightly simplified by substituting the six perypherical ethyl substituents with hydrogen atoms.

**Synthesis of 2**: $FeCl_2(THF)_{1.5}$ (11.9 g, 50.7 mmol) was added to a solution of $Li_2(Et_6Py_4)(THF)_2$ (32.28 g, 50.7 mmol) in benzene (400 mL). The solution was stirred overnight at room temperature and then refluxed for 3 h. Lithium chloride was filtered off, the resulting orange solution was evaporated to dryness, and *n*-hexane (120 mL) was added to give a brown powder, which was collected and dried in vacuo (17.59 g, 65 %). Green crystals suitable for X-ray analysis were isolated from toluene/hexane. $\mu_{eff}$ (298 K) = 3.69 $\mu_B$; IR (nujol): $\tilde{\nu}$ = 1579.1 (s, methene), 1464.8 (s), 1387.0 (s), 1322.2 (m), 1292.6 (s), 1243.1 (s), 1063.7 (s), 1022.8 (s), 846.2 (m), 774.3 (m), 756.2 (w), 724.6 (m), 693.9 $cm^{-1}$ (w); UV/Vis ($C_6H_6$): $\lambda_{max}$ ($\varepsilon$) = 448 nm (43 700 $mol^{-1} dm^3 cm^{-1}$); elemental analysis (%) calcd for $C_{32}H_{38}FeN_4$: C 71.90, H 7.17, N 10.48; found C 72.09, H 7.19, N 9.55.

**Synthesis of 3**: $FeCl_2(THF)_{1.5}$ (0.44 g, 1.87 mmol) was added to a solution of $Li_2(Et_6Py_4)(THF)_2$ (1.20 g, 1.88 mmol) in benzene (100 mL). The solution was stirred overnight at room temperature and subsequentially refluxed for 3 h. Lithium chloride was filtered off, the resulting orange solution was evaporated to dryness, and THF (20 mL) was added. The yellow-orange solution was stirred for 2 h and *n*-hexane (100 mL) was added dropwise. The product was collected and dried in vacuo (0.82 g, 64 %). IR (nujol): $\tilde{\nu}$ = 1577.9 (s, methene), 1488.9 (w), 1463.4 (m), 1376.6 (m), 1301.7 (m), 1243.5 (m), 1062.6 (s), 1018.3 (s), 944.4 (w), 844.0 (m), 772.2 (w), 724.0 $cm^{-1}$ (m); UV/Vis (THF): $\lambda_{max}$ ($\varepsilon$) = 448 (76 200), 494 nm (sh, 10 400 $mol^{-1} dm^3 cm^{-1}$); elemental analysis (%) calcd for $C_{40}H_{54}FeN_4O_2$: C 70.78, H 8.02, N 8.25; found C 70.96, H 7.86, N 8.19.

**Synthesis of 4**: A solution of **2** (1.11 g, 2.08 mmol) in benzene (100 mL) was treated with an excess of pyridine (1.47 g, 18.6 mmol). The solution was stirred overnight at room temperature. The solvent was evaporated to dryness, and *n*-hexane (70 mL) was added to give a purple powder, which was collected and dried in vacuo (1.01 g, 70 %). Recrystallization of the powder from THF/hexane gave crystals that were suitable for X-ray analysis. $^1$H NMR (400 MHz, $C_6D_6$, 298 K): $\delta$ = 8.51 (d, 4H; $C_5H_5N$), 8.33 (d, $J$ = 4.0 Hz, 4H; $C_4H_2N$), 7.43 (d, $J$ = 4.0 Hz, 4H; $C_4H_2N$,), 7.04 (m, 2H; $C_5H_5N$), 6.71 (m, 4H; $C_5H_5N$), 2.74 (q, $J$ = 6.8 Hz, 4H; $CH_2$), 1.48 (q, $J$ = 6.8 Hz, 8H; $CH_2$), 1.03 (t, $J$ = 6.8 Hz, 6H; $CH_3$), 0.87 (t, $J$ = 6.8 Hz, 12H; $CH_3$); $^{13}$C NMR (50 MHz, $C_5D_5N$, 298 K): $\delta$ = 172.7, 147.9, 146.3, 139.3, 133.5, 126.3, 121.5, 48.0, 32.3, 25.2, 16.4, 8. 8; IR (nujol): $\tilde{\nu}$ = 1573.1 (s, methene), 1490.2 (m), 1455.6 (m), 1433.3 (m), 1373.6 (m), 1321.1 (s), 1277.3 (m), 1240.0 (m), 1195.5 (w), 1144.1 (w), 1063.4 (s), 987.4 (s), 837.8 (s), 767.6 (w), 717.1 (s), 692.1 $cm^{-1}$ (m); UV/Vis ($C_5H_5N$): $\lambda_{max}$ ($\varepsilon$) = 454 (69 000), 492 nm (sh, 14 400 $mol^{-1} dm^3 cm^{-1}$); elemental analysis (%) calcd for $C_{42}H_{48}FeN_6$: C 72.82, H 6.98, N 12.13; found C 72.60, H 7.18, N 11.92.

**Reaction of 2 with carbon monoxide to give complex 5**: A solution of **2** (1.5 g, 2.8 mmol) in toluene (200 mL) was exposed to a CO atmosphere for 2 d at room temperature. IR (solution in toluene): $\tilde{\nu}$ = 2021.6 (s), 1586.4 (s, methene), 1456.6 (m), 1325.4 (s), 1245.8 (m), 1072.7 (s), 999.4 (s), 843.0 $cm^{-1}$ (m). Toluene was evaporated from the reaction mixture, and the remaining residue was collected with *n*-hexane (90 mL), yielding a brown powder. Recrystallization from toluene/hexane gave crystals of **2**.

**Synthesis of 6**: A solution of **2** (1.17 g, 2.19 mmol) and pyridine (0.17 g, 2.15 mmol) in toluene (50 mL) was exposed to a CO atmosphere for 1 d at room temperature. The solvent was evaporated, and the red-orange solid was triturated with *n*-hexane (50 mL) and then dried in vacuo (0.92 g, 66 %). Recrystallization of the powder from toluene/hexane gave dark red crystals that were suitable for X-ray analysis. $^1$H NMR (400 MHz, $C_6D_6$, 298 K): $\delta$ = 7.69 (d, 2H; $C_5H_5N$), 7.37 (d, 4H; $C_4H_2N$), 6.60 (d, 4H; $C_4H_2N$), 6.45 (m, 1H; $C_5H_5N$), 6.16 (m, 2H; $C_5H_5N$), 2.74 (q, $J$ = 6.8 Hz, 4H; $CH_2$), 2.29 (q, $J$ = 6.8 Hz, 4H; $CH_2$), 1.90 (q, $J$ = 6.8 Hz, 4H; $CH_2$), 1.08 (t, $J$ = 6.8 Hz, 6H; $CH_3$), 0.93 (t, $J$ = 6.8 Hz, 6H; $CH_3$), 0.80 (t, $J$ = 6.8 Hz, 6H; $CH_3$); $^{13}$C NMR (50 MHz, $C_5D_5N$, 298 K): $\delta$ = 222.5, 161.9, 147.8, 145.4, 143.3, 133.4, 126.7, 121.6, 115.8, 46.3, 34.7, 30.2, 24.5, 16.8, 8.4, 8.1; IR (nujol): $\tilde{\nu}$ = 1951.6 (m), 1582.3 (m, methene), 1461.3 (m), 1391.5 (w), 1346.7 (w), 1260.5 (m), 1133.6 (m), 1015.2 (m), 799.5 $cm^{-1}$ (m); UV/Vis ($C_5H_5N$): $\lambda_{max}$ ($\varepsilon$) = 446 (60 900), 462 nm (57 400 $mol^{-1} dm^3 cm^{-1}$); elemental analysis (%) calcd for $C_{38}H_{43}FeN_5O$: C 71.13, H 6.75, N 10.91; found C 70.32, H 6.79, N 10.92.

**Synthesis of 7**: *t*BuNC (0.36 g, 4.33 mmol) was added to a solution of **2** (1.15 g, 2.15 mmol) in toluene (75 mL), and the mixture was stirred overnight at room temperature. The color changed from orange to yellow-green. The solvent was evaporated to dryness, and the residue was treated with *n*-hexane (75 mL), collected, and dried in vacuo (0.88 g, 58 %). Recrystallization from toluene/hexane produced crystals of **6** that were suitable for X-ray analysis. $^1$H NMR (200 MHz, $C_6D_6$, 298 K): $\delta$ = 7.60 (d, $J$ = 4.4 Hz, 4H; $C_4H_2N$), 6.75 (d, $J$ = 4.4 Hz, 4H; $C_4H_2N$), 3.02 (q, $J$ = 7.2 Hz, 4H; $CH_2$), 2.25 (q, $J$ = 7.2 Hz, 8H; $CH_2$), 1.39 (t, $J$ = 7.2 Hz, 6H; $CH_3$), 0.97 (t, $J$ = 7.2 Hz, 12H; $CH_3$), 0.69 (s, 18H; $CH_3$); $^{13}$C NMR (50 MHz, $C_6D_6$, 298 K): $\delta$ = 187.8, 169.6, 164.1, 142.7, 136.6, 116.3, 48.9, 36.7, 27.3, 19.0, 11.0; IR (nujol): $\tilde{\nu}$ = 2113.3 (m), 1594.2 (s, methene), 1331.0 (s), 1082.1 (s), 1071.7 (s), 1057.1 (m), 1049.2 (m), 988.3 (m), 922.3 (m), 911.6 (m), 905.1 (m), 899.9 $cm^{-1}$ (w); UV/Vis ($C_6H_6$): $\lambda_{max}$ ($\varepsilon$) = 448 (82 600), 484 nm (sh, 24 600 $mol^{-1} dm^3 cm^{-1}$); elemental analysis (%) calcd for $C_{42}H_{56}FeN_6$: C 71.98, H 8.05, N 11.99; found C 71.95, H 8.17, N 11.94.

**Synthesis of 8**: $Bu_4NCN(THF)$ (0.66 g, 1.94 mmol) was added to a solution of **2** (1.04 g, 1.95 mmol) in benzene (120 mL). The color immediately changed from orange to yellow. The solution was stirred overnight at room temperature. The solvent was evaporated to dryness, and the yellow residue was then treated with *n*-hexane (75 mL); this resulted in a suspension from which a yellow product was collected and dried in vacuo (0.95 g, 61 %). Recrystallization of the powder from DME/hexane gave crystals that were suitable for X-ray analysis. $\mu_{eff}$ (298 K) = 4.72 $\mu_B$; IR (nujol): $\tilde{\nu}$ = 2049.2 (m), 1571.9 (s, methene), 1458.9 (s), 1376.3 (m), 1301.7 (s), 1240.9 (s), 1063.9 (s), 994.3 (s), 843.3 (m), 768.5 (m), 748.4 (m), 722.2 $cm^{-1}$ (m); UV/Vis ($C_6H_6$): $\lambda_{max}$ ($\varepsilon$) = 458 (83 300), 506 nm sh (6000 $mol^{-1} dm^3 cm^{-1}$); elemental analysis (%) calcd for $C_{49}H_{74}FeN_6$: C 73.29, H 9.29, N 10.47; found C 72.68, H 9.50, N 10.03.

**Synthesis of 9**: Pyridine (0.15 g, 1.90 mmol) was added to a solution of **8** (0.95 g, 1.18 mmol) in THF (120 mL). The mixture was stirred overnight at room temperature. The solvent was evaporated to dryness, and *n*-hexane (60 mL) was added to give a yellow-orange powder, which was collected and dried in vacuo (0.49 g, 47 %). Recrystallization from THF/*n*-hexane gave crystals that were suitable for X-ray analysis. $^1$H NMR (400 MHz, $C_6D_6$, 298 K): $\delta$ = 8.51 (br s, 2H; $C_5H_5N$), 8.33 (d, $J$ = 4 Hz, 4H; $C_4H_2N$), 7.43 (d, $J$ = 4 Hz, 4H; $C_4H_2N$), 7.05 (m, 1H; $C_5H_5N$), 6.73 (m, 2H; $C_5H_5N$), 3.34 (m, 8H; $NCH_2-$), 2.88 (q, $J$ = 7.2 Hz, 4H; $CH_2$), 2.73 (q, $J$ = 7.2 Hz, 4H; $CH_2$), 2.46 (q, $J$ = 7.2 Hz, 4H; $CH_2$), 1.65 (m, 8H; $CH_2$), 1.37 (m, 8H; $CH_2$), 1.27 (t, $J$ = 7.2 Hz, 6H; $CH_3$), 1.15 (t, $J$ = 7.2 Hz, 6H; $CH_3$), 1.06 (t, $J$ = 7.2 Hz, 6H; $CH_3$), 0.96 (m, 12H; $CH_3$); $^{13}$C NMR (50 MHz, $C_5D_5N$, 298 K,): $\delta$ = 215.7, 165.7, 148.2, 146.2, 139.4, 133.9, 131.7, 126.4, 121.8, 56.8, 46.4, 33.9, 30.3, 25.1, 22.2, 18.0, 16.3, 11.8, 9.2, 9.0; IR (nujol): $\tilde{\nu}$ = 1965.8 (w), 1575.6 (m, methene), 1462.8 (s), 1368.8 (w), 1260.7 (m), 1091.5 (m), 1035.0 (m), 800.0 $cm^{-1}$ (w)[1]; UV/Vis ($C_5H_5N$): $\lambda_{max}$ ($\varepsilon$) = 454 (79 500), 492 nm (sh, 16 800 $mol^{-1} dm^3 cm^{-1}$); elemental analysis (%) calcd for $C_{54}H_{79}FeN_7$: C 73.53, H 9.03, N 11.11; found C 73.27, H 8.69, N 10.83. The crystals used for the X-ray analysis contain an additional mole of pyridine.

**Synthesis of 10**: A solution of **2** (2.18 g, 4.08 mmol) in benzene (100 mL) was treated with an excess of iodobenzene dichloride (1.17 g, 4.26 mmol). The color changed immediately from orange to brown. The solution was stirred overnight at room temperature. Benzene was evaporated from the reaction mixture, and the remaining dark brown residue was collected with *n*-hexane (80 mL), yielding a brown powder (1.83 g, 79 %). Recrystallization from DME/hexane gave crystals that were suitable for X-ray analysis. $\mu_{eff}$ (290 K) = 5.55 $\mu_B$; IR (nujol): $\tilde{\nu}$ = 1587.1 (s, methene), 1464.7 (m), 1377.6 (m), 1314.2 (m), 1232.6 (s), 1072.3 (s), 1013.2 (s), 844.6 $cm^{-1}$ (m); UV/Vis ($C_6H_6$): $\lambda_{max}$ ($\varepsilon$) = 388 (43 700), 438 (55 400), 480 nm (39 300 $mol^{-1} dm^3 cm^{-1}$); elemental analysis (%) calcd for $C_{32}H_{38}ClFeN_4$: C 67.43, H 6.72, N 9.83; found C 67.77, H 7.15, N 9.97.

**Synthesis of 11 (method A)**: A solution of **2** (1.21 g, 2.26 mmol) in toluene (200 mL) was exposed to dry oxygen for 1 d at room temperature. The color changed from orange to red-orange. Toluene was evaporated from the reaction mixture, and the remaining residue was collected with *n*-hexane (100 mL), yielding a brown-orange powder (1.15 g, 47 %). Crystals suitable for X-ray analysis were obtained by recrystallization in toluene/hexane. $\mu_{eff}$ (298 K) = 3.05 $\mu_B$; IR (nujol): $\tilde{\nu}$ = 1583.7 (s, methene), 1488.9 (w), 1465.4 (m), 1381.8 (m), 1327.8 (m), 1305.6 (m), 1290.3 (s), 1236.9 (s), 1064.9 (s), 1010.4 (s), 871.3 (m, Fe–O–Fe), 846.1 (m), 771.6 (m), 724.0 $cm^{-1}$ (m)[1]; elemental analysis (%) calcd for $C_{64}H_{76}Fe_2N_8O$: C 70.84, H 7.06, N 10.33;found C 71.11, H 7.78, N 9.75. A solution of **2** (0.83 g, 1.55 mmol) in toluene (100 mL) was exposed to dry oxygen. Gas volumetry showed that the solution absorbed 0.88 mmol of $O_2$ (70 min).

**Synthesis of 11 (method B)**: Iodosobenzene (0.89 g, 4.01 mmol) was added to a solution of **2** (2.04 g, 3.82 mmol) in benzene (100 mL). The mixture was stirred overnight at room temperature. The solvent was evaporated to dryness, and *n*-hexane (80 mL) was added to give a red powder, which was collected and dried in vacuo (0.64 g, 15%). Crystals suitable for X-ray analysis were obtained in toluene/hexane solution. $\mu_{eff}$ (298 K) = 3.05 $\mu_B$; IR (nujol): $\tilde{\nu}$ = 1583.7 (s, methene), 1488.9 (w), 1465.4 (m), 1381.8 (m), 1327.8 (m), 1305.6 (m), 1290.3 (s), 1236.9 (s), 1064.9 (s), 1010.4 (s), 871.3 (m, Fe−O−Fe), 846.1 (m), 771.6 (m), 724.0 $cm^{-1}$ (m)[1]; UV/Vis ($C_6H_6$): $\lambda_{max}$ ($\varepsilon$) = 364 (17600), 450 (31500), 482 nm (30500 $mol^{-1} dm^3 cm^{-1}$); elemental analysis (%) calcd for $C_{64}H_{76}Fe_2N_8O$: C 70.84, H 7.06, N 10.33; found C 70.76, H 7.14, N 10.16.

**Synthesis of 12**: *p*-Benzoquinone (0.135 g, 1.25 mmol) was added to a solution of **2** (1.35 g, 2.52 mmol)in benzene (150 mL), and the mixture was stirred overnight at room temperature. The color changed from orange to dark orange. Benzene was evaporated from the reaction mixture, and the remaining residue was collected with *n*-hexane (75 mL), yielding a dark purple powder (1.99 g, 67%). Recrystallization of the powder from THF/hexane gave crystals that were suitable for X-ray analysis. $\mu_{eff}$ (298 K) = 4.83 $\mu_B$; IR (nujol): $\tilde{\nu}$ = 1585.0 (s, methene), 1484.4 (m), 1461.1 (m), 1379.3 (m), 1318.5 (m), 1294.4 (m), 1272.2 (s), 1237.0 (s), 1072.2 (s), 1013.7 (m), 845.4 (m), 773.9 (w), 722.4 $cm^{-1}$ (w); UV/Vis ($C_6H_6$): $\lambda_{max}$ ($\varepsilon$) = 374 (27800), 450 (56100), 510 nm (26800 $mol^{-1} dm^3 cm^{-1}$); elemental analysis (%) calcd for $C_{70}H_{80}Fe_2N_8O_2$: C 71.42, H 6.85, N 9.52; found C 71.18, H 6.90, N 9.33.

**Synthesis of 13**: A solution of **2** (1.36 g, 2.41 mmol) in benzene (150 mL) was exposed to an NO atmosphere for 1 d at room temperature. Benzene was evaporated, and the dark brown solid was triturated with *n*-pentane (100 mL) and dried in vacuo (0.74 g, 52%). Crystals suitable for X-ray analysis from a benzene/hexane solution and were dark red. IR (nujol): $\tilde{\nu}$ = 1690.6 (s), 1581.7 (s, methene), 1461.6 (s), 1377.0 (m), 1297.6 (m), 1065.7 (s), 1017.1 (s), 799.0 (m), 720.0 $cm^{-1}$ (m); UV/Vis ($C_6H_6$): $\lambda_{max}$ ($\varepsilon$) = 464 nm (17000 $mol^{-1} dm^3 cm^{-1}$); elemental analysis (%) calcd for $C_{32}H_{38}FeN_5O$: C 68.08, H 6.78, N 12.41; found C 66.22, H 6.77, N 12.72.

**Synthesis of 14**: Nitrosobenzene (0.06 g, 0.56 mmol) and an excess of pyridine (0.1 g, 1.26 mmol) were added to a solution of **2** (0.28 g, 0.52 mmol) in benzene (120 mL). The solution was stirred overnight at room temperature. The solvent was evaporated to dryness, and the product was washed with *n*-hexane (40 mL), collected, and dried in vacuo (0.21 g, 58%). $^1$H NMR (200 MHz, $C_6D_6$, 298 K): $\delta$ = 7.84 (d, 2H; $C_6H_5NO$), 7.35 (d, $J$ = 4.4 Hz, 4H; CH), 7.13 (t, 1H; $C_6H_5NO$), 7.03 (d, 2H; $C_5H_5N$), 6.74 (t, 2H; $C_6H_5NO$), 6.48 (t, 1H; $C_5H_5N$), 6.38 (d, $J$ = 4.4 Hz, 4H; CH), 6.15 (t, 2H; $C_5H_5N$), 2.83 (q, $J$ = 7.2 Hz, 4H; $CH_2$), 1.92 (q, $J$ = 7.2 Hz, 4H; $CH_2$), 1.46 (q, $J$ = 7.2 Hz, 4H; $CH_2$), 1.14 (t, $J$ = 7.2 Hz, 6H; $CH_3$), 0.91 (t, $J$ = 7.2 Hz, 6H; $CH_3$), 0.33 (t, $J$ = 7.2 Hz, 6H; $CH_3$); $^{13}$C NMR (50 MHz, $C_6D_6$, 298 K): $\delta$ = 165.9, 160.4, 150.8, 145.4, 135.8, 130.6, 128.3, 128.1, 127.8, 122.7, 120.5, 116.8, 47.4, 37.1, 30.5, 26.7, 18.9, 10.8, 9.1; IR (nujol): $\tilde{\nu}$ = 1583.3 (s, methene), 1522.2 (w), 1494.4 (m), 1463.2 (s), 1376.9 (m), 1327.8 (s), 1318.2 (s), 1294.4 (s), 1238.9 (m), 1216.7 (w), 1200.0 (w), 1066.7 (s), 1006.8 (s), 844.6 (m), 767.9 (m), 719.3 (m), 694.4 $cm^{-1}$ (m); UV/Vis ($C_5H_5N$): $\lambda_{max}$ ($\varepsilon$) = 454 (33300), 506 nm (sh, 20000 $mol^{-1} dm^3 cm^{-1}$); elemental analysis (%) calcd for $C_{43}H_{48}FeN_6O$: C 71.66, H 6.71, N 11.66; found C 70.78, H 6.98, N 10.67.

**X-ray crystallography for complexes 2, 7, 8, 9, 11, 13, and 14**: Single crystals of **2**, **7**, **8**, **9**, **11**, **13**, and **14** were mounted in glass capillaries and sealed under nitrogen. Data concerning crystals, data collection, and structure refinement are listed in Table 1. For all complexes but **14**, the diffraction data were collected at 143 K on a mar345 imaging plate detector (60 images with a $\Delta\varphi$ of 3° and an exposure time of 3 min) and the data reduction was performed with marHKL release 1.9.1.[39] For complex **14**, data were collected on a KUMA diffractometer with kappa geometry, equipped with a CCD detector and were then reduced with CrysAlis.RED release 1.6.2.[40] The structure was solved and refined in space group $Pna2_1$; however, the absolute structure parameter[41] deviates from zero [0.40(2)]. No kind of absorption correction was applied to data sets. Structure solutions were determined with ab-initio direct methods.[42] All structures were refined using the full-matrix least-squares on $F^2$ with all non-H atoms anisotropically defined. H atoms were placed in calculated positions using the "riding model" with $U_{iso} = a\,U_{eq}$(C) (where $a$ is 1.5 for methyl hydrogens and 1.2 for others, while C is the parent carbon atom). One problem was encountered during the refinement of **9** and it dealt with disorder shown by one butyl group of the $N(tBu)_4^+$. The disorder was solved by splitting two atoms of the butyl chain (C45 and C46) into two staggered positions (A and B) with occupancy factors of 0.715(12) (A) and 0.285(12) (B) and by applying geometrical restraints involving the distance between them. Structure refinement, molecular graphics, and geometrical calculation were carried out on all structures with the SHELXTL software package, release 5.1.[27] Crystallographic data (excluding structure factors) for the structures reported in this paper have been deposited with the Cambridge Crystallographic Data Centre as supplementary publication no. CCDC-143082 – CCDC-143088, CCDC-146595, and CCDC-146596. Copies of the data can be obtained free of charge on application to CCDC, 12 Union Road, Cambridge CB2 1EZ, UK (fax: (+44) 1223-336-033; e-mail: deposit@ccdc.cam.ac.uk).

## Acknowledgement

We thank the "Fonds National Suisse de la Recherche Scientifique" (Bern, Switzerland, Grant No. 20 – 53336.98), Action COST D9 (European Program for Scientific Research, OFES No. C98.008), and Fondation Herbette (University of Lausanne, N. Re) for financial support.

[1] a) D. Mauzerall, S. Granick, *J. Biol. Chem.* **1958**, *232*, 1141; b) R. B. Woodward, *Angew. Chem.* **1960**, *72*, 651; c) A. Treibs, H. Häberle, *Justus Liebigs Ann. Chem.* **1968**, *718*, 183; d) D. Dolphin, *J. Heterocycl. Chem.* **1970**, *7*, 275.

[2] a) *The Porphyrins*, *Vol. 1* (Ed.: D. Dolphin), Academic Press, New York, **1978**, Chapter 3; b) *The Porphyrins*, *Vol. 2* (Ed.: D. Dolphin), Academic Press, New York, **1978**, Chapters 1 and 2; c) F.-P. Montforts, B. Gerlach, F. Höper, *Chem. Rev.* **1994**, *94*, 327.

[3] a) A. Botulinski, J. W. Buchler, M. Wicholas, *Inorg. Chem.* **1987**, *26*, 1540; b) J. W. Buchler, L. Puppe, *Justus Liebigs Ann. Chem.* **1970**, *740*, 142; c) J. W. Buchler, K. L. Lay, P. D. Smith, W. R. Scheidt, G. A. Ruppzecht, J. E. Kenny, *J. Organomet. Chem.* **1976**, *110*, 109; d) J. W. Buchler, C. Dreher, K. L. Lay, Y. J. A. Lee, W. R. Scheidt, *Inorg. Chem.* **1983**, *22*, 888; e) J. W. Buchler, K. L. Lay, Y. J. A. Lee, W. R. Scheidt, *Angew. Chem.* **1982**, *94*, 456; *Angew. Chem. Int. Ed. Engl.* **1982**, *21*, 432; f) P. N. Dwyer, J. W. Buchler, W. R. Scheidt, *J. Am. Chem. Soc.* **1974**, *96*, 2789; g) D. Mauzerall, *J. Am. Chem. Soc.* **1962**, *84*, 2437; h) M. W. Renner, J. W. Buchler, *J. Phys. Chem.* **1995**, *99*, 8045; i) P. N. Dwyer, L. Puppe, J. W. Buchler, W. R. Scheidt, *Inorg. Chem.* **1975**, *14*, 1782; j) A. Botulinski, J. W. Buchler, Y. J. A. Lee, W. R. Scheidt, *Inorg. Chem.* **1988**, *27*, 927; k) A. Botulinski, J. W. Buchler, B. Tonn, M. Wicholas, *Inorg. Chem.* **1985**, *24*, 3239.

[4] V. Kràl, J. L. Sessler, R. S. Zimmerman, D. Seidel, V. Linch, B. Andreoletti, *Angew. Chem.* **2000**, *112*, 1097; *Angew. Chem. Int. Ed.* **2000**, *39*, 1055.

[5] a) J.-M. Benech, E. Solari, L. Bonomo, R. Scopelliti, C. Floriani, *Angew. Chem.* **1999**, *111*, 2107; *Angew. Chem. Int. Ed.* **1999**, *38*, 1957; b) L. Bonomo, E. Solari, R. Scopelliti, C. Floriani, N. Re, *J. Am. Chem. Soc.* **2000**, *122*, 5312.

[6] Some porphodimetheneiron(III) complexes are in refs. [3e,j].

[7] a) *The Porphyrin Handbook*, *Vol. 3* (Eds.: K. M. Kadish, K. M. Smith, R. Guilard), Academic Press, Burlington, MA, **1999**, Chapter 15; b) *The Porphyrin Handbook*, *Vol. 3* (Eds.: K. M. Kadish, K. M. Smith, R. Guilard), Academic Press, Burlington, MA, **1999**, Chapter 16; c) *The Porphyrin Handbook*, *Vol. 4* (Eds.: K. M. Kadish,K. M. Smith, R. Guilard), Academic Press, Burlington, MA, **1999**, Chapter 26; d) *The Porphyrin Handbook*, *Vol. 4* (Eds.: K. M. Kadish, K. M. Smith, R. Guilard), Academic Press, Burlington, MA, **1999**, Chapter 27; e) *The Porphyrin Handbook*, *Vol. 4* (Eds.: K. M. Kadish,K. M. Smith, R. Guilard), Academic Press, Burlington, MA, **1999**, Chapter 28.

[8] a) J. P. Collmann, J. L. Hoard, N. Kim, G. Lang, C. A. Reed, *J. Am. Chem. Soc.* **1975**, *97*, 2676; b) S. H. Strauss, M. E. Silver, K. M. Long, R. G. Thompson, R. A. Hudgens, K. Spartalian, J. A. Ibers, *J. Am. Chem. Soc.* **1985**, *107*, 4207; c) N. Li, Z. Su, P. Coppens, J. Landrum, *J. Am. Chem. Soc.* **1990**, *112*, 7294; d) M. P. Byrn, C. J. Curtis, I. Goldberg, Y. Hsiou, S. I. Khan, P. A. Sawin, S. K. Tendick, C. E. Strouse, *J. Am. Chem. Soc.* **1991**, *113*, 6549.

[9] a) S-M. Peng, J. A. Ibers, *J. Am. Chem. Soc.* **1976**, *98*, 8032; b) R. Salzmann, C. J. Ziegler, N. Godbout, M. T. McMahon, K. S. Suslick, E.

  0947-6539/00/0624-4530 $ 17.50+.50/0 *Chem. Eur. J.* **2000**, *6*, No. 24

Oldfield, *J. Am. Chem. Soc*. **1998**, *120*, 11323; c) R. Salzmann, M. T. McMahon, N. Godbout, L. K. Sanders, M. Wojdelski, E. Oldfield, *J. Am. Chem. Soc*. **1999**, *121*, 3818.
[10] G. B. Jameson, J. A. Ibers, *Inorg. Chem*. **1979**, *18*, 1200.
[11] a) W. R. Scheidt, Y. J. Lee, W. Luangdilok, K. J. Haller, K. Anzai, K. Hatano, *Inorg. Chem*. **1983**, *22*, 1516; b) W. R. Scheidt, K. Hatano, *Acta Crystallogr. Sect. C* **1991**, *47*, 2201.
[12] N. Godbout, L. K. Sanders, R. Salzmann, R. H. Havlin, M. Wojdelski, E. Oldfield, *J. Am. Chem. Soc*. **1999**, *121*, 3829.
[13] a) W. R. Scheidt, K. J. Haller, K. Hatano, *J. Am. Chem. Soc*. **1980**, *102*, 3017; b) M. J. Scott, S. C. Lee, R. H. Holm, *Inorg. Chem*. **1994**, *33*, 4651.
[14] a) W. R. Scheidt, M. G. Finnegan, *Acta Crystallogr*. Sect. *C*, **1989**, *45*, 1214; b) R.-J. Cheng, P.-Y. Chen, P.-R. Gau, C.-C. Chen, S.-M. Peng, *J. Am. Chem. Soc*. **1997**, *119*, 2563; c) M. Mazzanti, J.-C. Marchon, J. Wojaczynski, S. Wolowiec, L. Latos-Grazynski, M. Shang, W. R. Scheidt, *Inorg. Chem*. **1998**, *37*, 2476; d) T. Ikeue, Y. Ohgo, A. Uchida, M. Nakamura, H. Fujii, M. Yokohama, *Inorg. Chem*. **1998**, *38*, 1276, **1999**.
[15] a) B. Cheng, J. D. Hobbs, P. G. Debrunner, J. Erlebacher, J. A. Shellnutt, W. R. Scheidt, *Inorg. Chem*. **1995**, *34*, 102; b) K. D. Karlin, A. Nanthakumar, S. Fox, N. N. Murthy, N. Ravi, B. H. Huynh, R. D. Orosz, E. P. Day, *J. Am. Chem. Soc*. **1994**, *116*, 4753; c) K.-L. Lay, J. W. Buchler, J. E. Kenny, W. R. Scheidt, *Inorg. Chim. Acta* **1986**, *123*, 91; d) A. Gold, K. Jayaraj, P. Doppelt, J. Fischer, R. Weiss, *Inorg. Chim. Acta* **1988**, *150*, 177; e) A. U. Hoffman, D. M. Collins, V. W. Day, E. B. Fleischer, T. S. Srivastava, J. L.Hoard, *J. Am. Chem. Soc*. **1972**, *94*, 3620; f) S. H. Strauss, M. J. Pawlik, J. Skowyra, J. R. Kennedy, O. P. Anderson, K. Spartalian, J. L. Dye, *Inorg. Chem*. **1987**, *26*, 724.
[16] a) W. R. Scheidt, M. E. Frisse, *J. Am. Chem. Soc*. **1975**, *97*, 17; b) M. K. Ellison, W. R. Scheidt, *J. Am. Chem. Soc*. **1997**, *119*, 7404.
[17] M. K. Ellison, W. R. Scheidt, *J. Am. Chem. Soc.* **1997**, *119*, 7404.
[18] a) H. Scheer, H. H. Inhoffen, in *The Porphyrins Vol. 2* (Ed.: D. Dolphin), Academic Press, New York, **1978**, p. 45, and references therein; b) B. Tonn, Ph.D. thesis, Rheinisch-Westfälischen Technischen Hochschule, Aachen, Germany, **1979**.
[19] M. Gouterman, in *The Porphyrins*, *Vol. 3* (Ed.: D. Dolphin), Academic Press, New York, **1978**, Chapter 1.
[20] a) A. Botulinski, J. W. Buchler, K. L. Lay, J. Ensling, H. Twilfer, J. Billecke, H. Lueken, B. Tonn, *ACS Adv. Chem. Ser.* **1982**, *201*, 253–277; b) J. W. Buchler, K. L. Lay, *Z. Naturforsch. Teil B* **1975**, *30*, 385–392.
[21] H. Kobayashi, *Adv. Biophys. Chem.* **1975**, *8*, 191.
[22] C. G. Barraclough, R. L. Martin, S. Mitra, R. C. Sherwood, *J. Chem. Phys.* **1970**, *53*, 1643.
[23] P. W. D. Boyd, D. A. Buckingham, R. F. McMeeking, S. Mitra, *Inorg. Chem.* **1979**, *18*, 3585.
[24] a) O. Kahn, *Molecular Magnetism*, VCH, New York, **1993**; b) R. L. Carlin, *Magnetochemistry*, Springer, Berlin, **1986**; c) C. J. O'Connor, *Prog. Inorg. Chem.* **1982**, *29*, 203.
[25] W. R. Scheidt, C. A. Reed, *Chem. Rev.* **1981**, *81*, 543.
[26] W. R. Scheidt, M. Gouterman in *Iron Porphyrins* (Eds.: H. B. Gray, A. B. P. Lever), Addison-Wesley, Reading, MA, **1982**, p. 89.
[27] Bruker AXS, Madison, Wisconsin, 53719 (USA), **1997**.
[28] W. R. Scheidt, M. K. Ellison, *Acc. Chem. Res.* **1999**, *32*, 350.
[29] a) K. S. Murray, *Coord. Chem. Rev.* **1974**, *12*, 1; b) J. H. Helms, L. W. ter Haar, W. E. Hatfield, D. L. Harris, K. Jayaraj, G. E. Toney, A. Gold, T. D. Mewborn, J. R. Pemberton, *Inorg. Chem.* **1986**, *25*, 2334; c) H. Lueken, K. Handrick, H. Schilder, J. W. Buchler, K. L. Lay, *Z. Anorg. Allg. Chem.* **1996**, *622*, 95–99.
[30] H. Lueken, J. W. Buchler, K. L. Lay, *Z. Naturforsch. Teil B* **1976**, *31*, 1596–1603.
[31] A. Ghosh, *Acc. Chem. Res.* **1998**, *31*, 189.
[32] P. M. Kozlowski, T. G. Spiro, A. Bercés M. Z. Zgierski, *J. Phys. Chem. B* **1998**, *102*, 2603.
[33] R. Hoffmann, M. M. L. Chen, M. Elian, A. R. Rossi, D. M. P. Mingos, *Inorg. Chem.* **1974**, *16*, 2666.
[34] E. A. Boudreaux, L. N. Mulay, *Theory and Applications of Molecular Paramagnetism*, Wiley, New York, **1976** pp. 491–495.
[35] a) E. J. Baerends, D. E. Ellis, P. Ros, *Chem. Phys.* **1973**, *2*, 42; b) E. J. Baerends, P. Ros, *Chem. Phys.* **1973**, *2*, 51; c) E. J. Baerends, P. Ros, *Chem. Phys.* **1975**, *8*, 41; d) E. J. Baerends, P. Ros, *Int. J. Quantum Chem.* **1978**, *S12*, 169; d) P. M. Boerrigter, G. te Velde, E. J. Baerends, *Int. J. Quantum Chem.* **1988**, *33*, 87; e) G. te Velde, E. J. Baerends, *J. Comput. Phys.* **1992**, *99*, 84; e) T. Ziegler, V. Tschinke, E. J. Baerends, J. G. Snijders, W. Ravenek, *J. Phys. Chem.* **1989**, *93*, 3050.
[36] S. H. Vosko, L. Wilk, M. Nusair, *Can. J. Phys.* **1980**, *58*, 1200.
[37] A. D. Becke, *Phys. Rev.* **1988**, *A38*, 2398.
[38] J. P. Perdew, *Phys. Rev.* **1986**, *B33*, 8822.
[39] Z. Otwinowski, W. Minor, *Methods in Enzymology, Vol. 276: Macromolecular Crystallography*, *Part A* (Eds.: C. W. Carter, Jr., R. M. Sweet), Academic Press, New York, **1997**, pp. 307–326.
[40] Kuma Diffraction Instruments, PSE-EPFL module 3.4, Lausanne (Switzerland), **1999**.
[41] H. D. Flack, *Acta Crystallogr. Sect. A* **1983**, *39*, 876.
[42] G. M. Sheldrick, *Acta Crystallogr. Sect. A* **1990**, *46*, 467.

Received: April 14, 2000 [F2425]